REFERENCES

1. Sachs DH. The pig as a potential xenograft donor. *Pathol Biol* 1994; 42: 217.
2. Galili U. Interaction of the natural anti-Gal antibody with alpha-galactosyl epitopes: a major obstacle for xenotransplantation in humans. *Immunol Today* 1993; 14: 480.
3. Kolber-Simonds D, Lai L, Watt SR, et al. Production of a-1,3-galactosyltransferase null pigs by means of nuclear transfer with fibroblasts bearing loss of heterozygosity mutations. *Proc Natl Acad Sci U S A* 2004; 101: 7335.
4. Dai Y, Vaught TD, Boone J, et al. Targeted disruption of the alpha1,3-galactosyltransferase gene in cloned pigs. *Nat Biotechnol* 2002; 20: 251.
5. Westall GP, Levvey BJ, Salvaris E, et al. Sustained function of genetically modified porcine lungs in an ex vivo model of pulmonary xenotransplantation. *J Heart Lung Transplant* 2013; 32: 1123.
6. Bauer A, Postrach J, Thormann M, et al. First experience with heterotopic thoracic pig-to-baboon cardiac xenotransplantation. *Xenotransplantation* 2010; 17: 243.
7. Fisicaro N, Londrigan SL, Brady JL, et al. Versatile co-expression of graft-protective proteins using 2A-linked cassettes. *Xenotransplantation* 2011; 18: 121.
8. Yamada K, Yazawa K, Shimizu A, et al. Marked prolongation of porcine renal xenograft survival in baboons through the use of a-1,3-galactosyltransferase gene-knockout donors and the cotransplantation of vascularized thymic tissue. *Nat Med* 2005; 11: 32.
9. Griesemer AD, Hirakata A, Shimizu A, et al. Results of Gal-Knockout Porcine Thymokidney Xenografts. *Am J Transplant* 2009; 12: 2669.
10. Chen G, Qian H, Starzl T, et al. Acute rejection is associated with antibodies to non-Gal antigens in baboons using Gal-knockout pig kidneys. *Nat Med* 2005; 11: 1295.
11. Pintore L, Paltrinieri S, Vadori M, et al. Clinicopathological findings in non-human primate recipients of porcine renal xenografts: quantitative and qualitative evaluation of proteinuria. *Xenotransplantation* 2013; 20: 449.
12. Shimatsu Y, Yamada K, Horii W, et al. Production of cloned NIBS (Nippon Institute for Biological Science) and alpha-1, 3-galactosyltransferase knockout MGH miniature pigs by somatic cell nuclear transfer using the NIBS breed as surrogates. *Xenotransplantation* 2013; 20: 157.
13. Fujimura T, Takahagi Y, Shigehisa T, et al. Production of alpha 1,3-galactosyltransferase gene-deficient pigs by somatic cell nuclear transfer: a novel selection method for gal alpha 1,3-Gal antigen-deficient cells. *Mol Reprod Dev* 2008; 75: 1372.
14. Yamada K, Tasaki M, Sekijima M, et al. Porcine Cytomegalovirus infection is associated with early rejection of kidney grafts in a pig to baboon xenotransplantation model. *Transplantation* 2014; 98: 411.
15. Mueller NJ, Barth RN, Yamamoto S, et al. Activation of cytomegalovirus in pig-to-primate organ xenotransplantation. *J Virol* 2002; 76: 4734.
16. Dzabic M, Rahbar A, Yaiw KC, et al. Intragraft cytomegalovirus protein expression is associated with reduced renal allograft survival. *Clin Infect Dis* 2011; 53: 969.
17. Mueller NJ, Sulling K, Gollackner B, et al. Reduced efficacy of ganciclovir against porcine and baboon cytomegalovirus in pig-to-baboon xenotransplantation. *Am J Transplant* 2003; 3: 1057.
18. Gollackner B, Mueller NJ, Houser S, et al. Porcine cytomegalovirus and coagulopathy in pig-to-primate xenotransplantation. *Transplantation* 2003; 75: 1841.
19. Li Y, Yan H, Xue WJ, et al. Allograft rejection-related gene expression in the endothelial cells of renal transplantation recipients after cytomegalovirus infection. *J Zhejiang Univ Sci B* 2009; 10: 820.
20. Kloover JS, Soots AP, Krogerus LA, et al. Rat cytomegalovirus infection in kidney allograft recipients is associated with increased expression of intracellular adhesion molecule-1 vascular adhesion molecule-1, and their ligands leukocyte function antigen-1 and very late antigen-4 in the graft. *Transplantation* 2000; 69: 2641.
21. Bishop GA, Hall BM. Expression of leucocyte and lymphocyte adhesion molecules in the human kidney. *Kidney Int* 1989; 36: 1078.
22. von Willebrand E, Pettersson E, Ahonen J, et al. CMV infection, class II antigen expression, and human kidney allograft rejection. *Transplantation* 1986; 42: 364.
23. Johnson J, Anderson B, Pass RF. Prevention of maternal and congenital cytomegalovirus infection. *Clin Obstet Gynecol* 2012; 55: 521.
24. Benoist G, Leruez-Ville M, Magny JF, et al. Management of pregnancies with confirmed cytomegalovirus fetal infection. *Fetal Diagn Ther* 2013; 33: 203.

A comparison of the main structures of N-glycans of porcine islets with those from humans

Shuji Miyagawa[1,2], Akira Maeda[2], Takuji Kawamura[2], Takehisa Ueno[2], Noriaki Usui[2], Sachiko Kondo[3], Shinichi Matsumoto[4], Teru Okitsu[5], Masafumi Goto[6], and Hiroshi Nagashima[7]

[2]Division of Organ Transplantation, Department of Surgery, Osaka University Graduate School of Medicine, Osaka, Japan; [3]GLYENCE Co., Ltd., Aichi, Japan; [4]National Center for Global Health and Medicine, Tokyo, Japan; [5]Institute of Industrial Science, University of Tokyo, Tokyo, Japan; [6]Tohoku University International Advanced Research and Education Organization, Tohoku University, Miyagi, Japan; and [7]Laboratory of Developmental Engineering, Department of Life Science, Meiji University, Kanagawa, Japan

After producing α1-3-galactosyltransferase knockout (GKO) pigs, most of the organs of these pigs showed less antigenicity to the human body. However, wild-type adult pig islets (API) that originally contained negligible levels of α-galactosidase now showed a clear antigenicity to human serum. In this study, N-glycans were isolated from both APIs and human islets. Their structures were then analyzed by a mapping technique based on their high-performance liquid chromatography elution positions and matrix-assisted laser desorption/ionization-time-of-flight -mass spectrometric data. Both preparations contained substantial amounts of high-mannose structures. The N-glycans from human islets were separated into 17 neutral, 8 mono-sialyl and 4 di-sialyl glycans, and the API glycans were comprised of 11 neutral, 8 mono-sialyl, 3 di-sialyl, 2 mono-sulfated, 3 mono-sialyl-mono-sulfated and 1 di-sulfated glycans. Among them, the API preparation contained one neutral, five mono-sialyl glycans and six sulfated glycans that were not detected in human islets. The structures of 9 of these 12 could be clearly determined. In addition, a study of the sulfate-depleted API suggests that sulfate residues could be antigenic to humans. The data herein will be helpful for future studies of the antigenicity associated with API.

Keywords: N-glycan / pig islets / sulfated glycan / xenotransplantation

[1]To whom correspondence should be addressed: e-mail: miyagawa@orgtrp.med.osaka-u.ac.jp

Introduction

The increasing challenges associated with the worldwide shortage of donor organs have led to a renewed interest in xenotransplantation. The pig pancreas is considered to be the most suitable source of islets for clinical xenotransplantation. Some clinical trials have resumed in New Zealand, Russia, etc., using islets from a wild-type pig via the use of an immuno-isolation technique (Elliott 2011). In addition, based on data collected from the "Inventory of human xenotransplantation practices" (http://www.humanxenotransplant.org/index.html), many clinical trials appear to be ongoing.

On the other hand, after producing α1-3-galactosyltransferase knockout (GKO) pigs (Dai et al. 2002; Takahagi et al. 2005), most of the organs from these pigs were found to show less antigenicity to the human body. However, wild-type adult pig islets (API) that originally contained negligible levels of α-galactosidase (α-Gal) (Galα1-3Gal) (Galili et al. 1987) showed a clear antigenicity to human serum (Komoda et al. 2004), and this fact represents a significant obstacle to successful xenotransplantation (Thompson et al. 2011).

Concerning the so-called non-Gal epitopes, many studies related to glycoproteins and glycolipids are on-going in attempts to identify them. However, our knowledge of non-Gal glycoantigens is still incomplete. That is, previous analyses of N-glycans from pigs included the use of additional tissues, in addition to islets. However, besides α-Gal and Hanganutziu-Deicher (Varki et al. 2009; Yamamoto et al. 2013) antigen expression, the glycosylation of API remains relatively unclear (Breimer 2011; Byrne et al. 2011; Miyagawa et al. 2012).

We wish to report herein on the analysis of the glycosylation of the N-linked sugars of API, compared with the corresponding values for human islets, using a high-performance liquid chromatography (HPLC) technique, which is capable of providing reliable data. The collected data will be of use in future research concerning non-Gal antigens and promises to provide us with clues for producing new types of immuno-modified pigs with less antigenicity than GKO pigs.

Results

Isolation of N-glycans of the porcine and human islets

N-glycans derived from porcine (11.9 mg of protein) and human islets (12.47 mg of protein) were separated into five peaks, based on increasing acidity using a diethylaminoethyl (DEAE) column. The following peaks were produced: Neutral
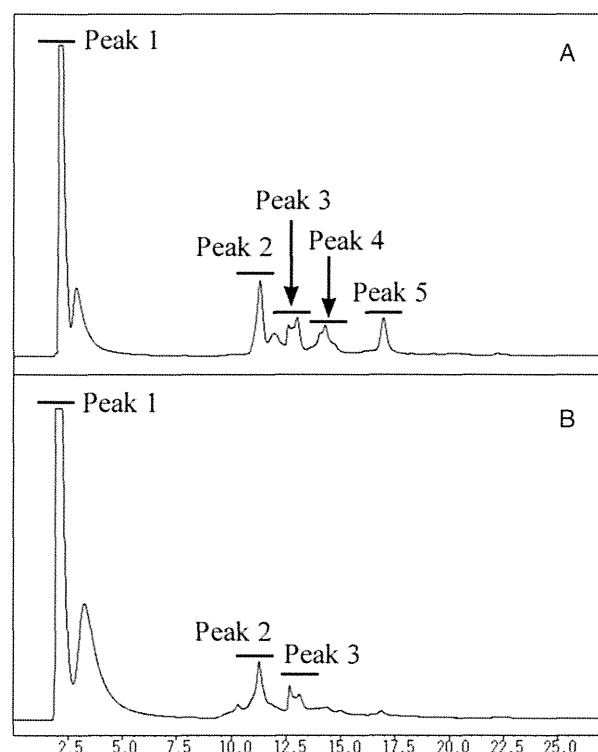
Fig. 1. Anion exchange DEAE elution profiles of PA-glycans derived from porcine islets (A) and the human islets (B). The PA-glycans were fractionated according to their sialic acid content and sulfate residues as neutral (Peak 1), mono-sialyl (Peak 2), di-sialyl or mono-sulfate (Peak 3), mono-sialyl-mono-sulfate (Peak 4) and di-sulfate (Peak 5) oligosaccharide fractions as indicated.

(N), Peak 1; mono-sialyl (M), Peak 2; di-sialyl (D) or mono-sulfate (S1), Peak 3; mono-sialyl-mono-sulfate (MS2), Peak 4 and di-sulfate (S2), Peak 5; glycan fractions with molar ratios (peak areas) of 84.4, 3.6, 2.6, 2.2 and 7.2% from APIs, and 94.0, 4.0, 2.0, 0 and 0% from the human islets, respectively (Figure 1).

Concerning API, when an octa decyl silyl (ODS) column was used, it was possible to separate the neutral fraction into fractions N1–N9, the mono-sialyl fraction into fractions M1–M6, the di-sialyl or mono-sulfate fraction into fractions D1–D3 and S1, the mono-sialyl-mono-sulfate fraction into fractions MS1–MS3 and the di-sulfate fraction into fraction S2. On the other hand, in the case of human islets, the neutral fraction was separated into N1–N13, the mono-sialyl into M1–M6 and the di-sialyl into D1–D4, as shown in Figure 2A–H.

Further analysis with GALAXY database

These ODS fractions were individually fractionated on an amide column and further subjected to matrix-assisted laser desorption/ionization time-of-flight mass spectrometric (MALDI-TOF-MS) analysis. The porcine N2, N6, M2, M3 and S1 and the human N2, N5, N6, N12, M2 and M4 fractions were found to contain two kinds of N-glycans (Figures 3 and 4).

The coordinates of all of the N-glycans coincided with those for known references in the glycoanalysis by the three axes of MS and chromatography (GALAXY) database except for several N-glycan fractions including human fractions N5-1, N5-2, N6-1, N6-2, M1, M2-2 and porcine S1-1, MS1and MS3. Most of the N-glycan structures were then identified by the mapping technique on the basis of their HPLC elution positions and MALDI-TOF-MS data.

Structural analysis of each sample

Pyridylamino (PA)-glycans, which did not correspond to any of the N-glycans so far registered in GALAXY, were trimmed by treatment with an exoglycosidase, which produced known glycans (Yagi et al. 2005).

In the case of S1-2, no reactivity was detected by β-acethyl-hexiominidase. Next, a methanolysis treatment induced the conversion of S1-2 into S1-2a, but additional treatment with β-galactosidase resulted in no change to S1-2a. Moreover, the β-N-acethylhexosaminidase treatment converted S1-2a into S1-2b, and S1-2b was proved to be the same structure as M4.1 in GALAXY, as evidenced by the observation that samples of S1-2b and M4.1 co-chromatographed (Figure 5).

The MS2 sample was analyzed following a similar procedure. The sample did not serve as a substrate for β-galactosidase and α2,3-sialydase, but was converted into MS2a by treatment with α-sialydase. Further methanolysis and β-galactosidase converted MS2a into MS2b and MS2c, respectively. MS2b was next verified to be 210.4a in GALAXY by the co-chromatography of both samples. On the other hand, MS2c, when treated with β-N-acethylhexosaminidase and methanolysis, was converted into MS2d and MS2e, respectively. MS2e was also proved to be 110.4a in GALAXY by the co-chromatography of both samples (Figure 6).

Concerning S2, the sample was unchanged as a result of a β-N-acethylhexosaminidase treatment. On the other hand, a methanolysis treatment cleaved two sulfate residues from S2 and produced S2a, which was shown to be 210.4b in GALAXY by the co-chromatography of both samples (Figure 7).

In the analyses, a total of 28 and 29 N-glycan structures of API and human islets, respectively, were identified and the findings are summarized in Tables I–VI (Supplementary data, Figure S1).

Sodium chlorate treatment on pig islets

The effect of removal of the sulfate structures of pig islets on the antigenicity to human serum was investigated. The use of a sodium chlorate and a sulfate-free medium led to a significant reduction in antigenicity to human serum, suggesting that the sulfate structures in adult islets are targets for human natural antibodies (Figure 8).

Discussion

Twenty-eight kinds of N-linked glycans were identified in the case of the API glycans and 29 were identified from human islets, based on their HPLC elution peaks. While the human preparation contained neutral, mono-sialyl, di-sialyl N-linked glycans, the API sample contained not only these three types, but mono-sulfate, MS2 and di-sulfate types of N-linked glycans
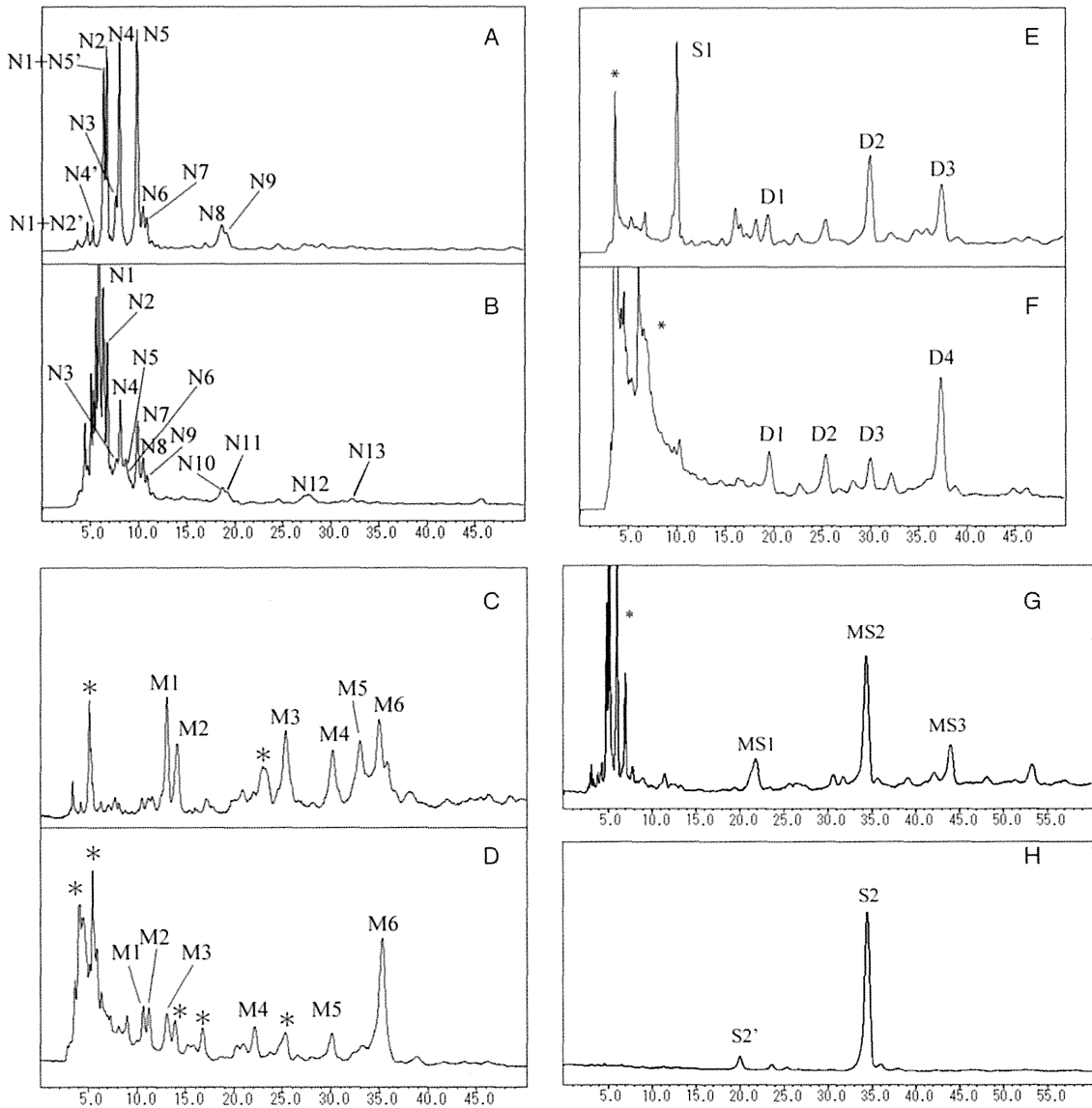
Fig. 2. Reverse-phase ODS elution profiles of PA-glycans obtained from each different fraction separated on the DEAE column. The neutral, mono-sialyl, di-sialyl or mono-sulfate, mono-sialyl-mono-sulfate and di-sulfate fractions were individually applied to the ODS column and gave elution profiles according to their hydrophobicity. (A) pig Peak 1, (B) human Peak 1, (C) pig Peak 2, (D) human Peak 2, (E) pig Peak 3, (F) human Peak 3, (G) pig Peak 4 and (H) pig Peak 5. N2': Epimerization of N2; N4': Epimerization of N4; N5': Epimerization of N5; S2': Epimerization of S2. Asterisks indicate the fractions containing no detectable PA-oligosaccharides.

as well. Among them, one neutral, five mono-sialyl and six sulfates of N-linked glycans in the API preparation were not detected in human islets. The structures of 9 of these 12 glycans were clearly identified in this study.

Concerning the characteristics of the N-glycans identified in the API preparation, the neutral glycans contained relatively high levels (%) of high-mannose type glycans. In comparison with the N-glycans from human islets, the high-mannose type of N-glycan found in API contains high levels (5 or 6) of

mannoses. In addition, glycans with structures of fractions N6-2 were not detected in human islets. On the other hand, in the case of API, the relative content of sulfated N-glycans approached 10%. In addition, the di-sulfate type glycans represented 7% of the relative quantity, indicating that sulfated N-glycans are a common structure in N-glycans of API but do not appear to be produced by human islets. In addition, all the sulfates are attached to a β-linked N-acetylgalactosamine (GalNAc).
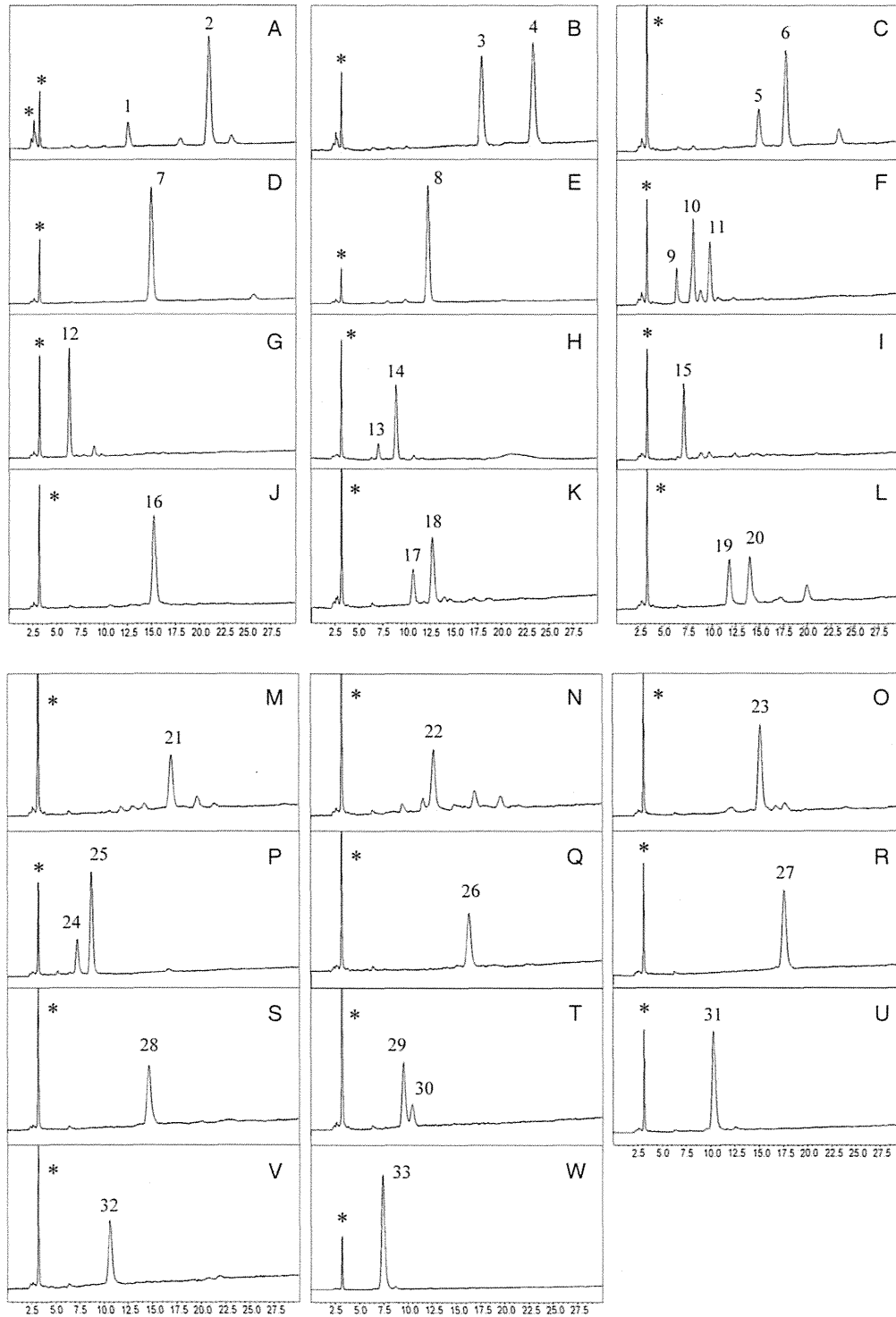
Fig. 3. Amide column elution profiles of PA-glycans of pig islets from each different fraction separated on the ODS column. (**A**) ODS peak-N1 + N5′. Peak 1 is the epimerization of the ODS peak-N5. Peak 2 was then settled as N1. (**B**) ODS peak-N2. Peaks 3 and 4 correspond to N2-1 and N2-2, respectively. (**C**) ODS peak-N3. Peak 5 was contamination of the ODS peak-N4. Peak 6 corresponds to N3. (**D**) ODS peak-N4. Peak 7 corresponds to N4. (**E**) ODS peak-N5. Peak 8 corresponds to N5. (**F**) ODS peak-N6. Peak 9 was contamination of ODS peak-N7. Peaks 10 and 11 correspond to N6-1 and N6-2, respectively. (**G**) ODS peak-N7. Peak 12 corresponds to N7. (**H**) ODS peak-N8. Peak 13 was contamination of ODS peak-N9. Peak 14 corresponds to N8. (**I**) ODS peak-N9. Peak 15 corresponds to N9. (**J**) ODS peak-M1.
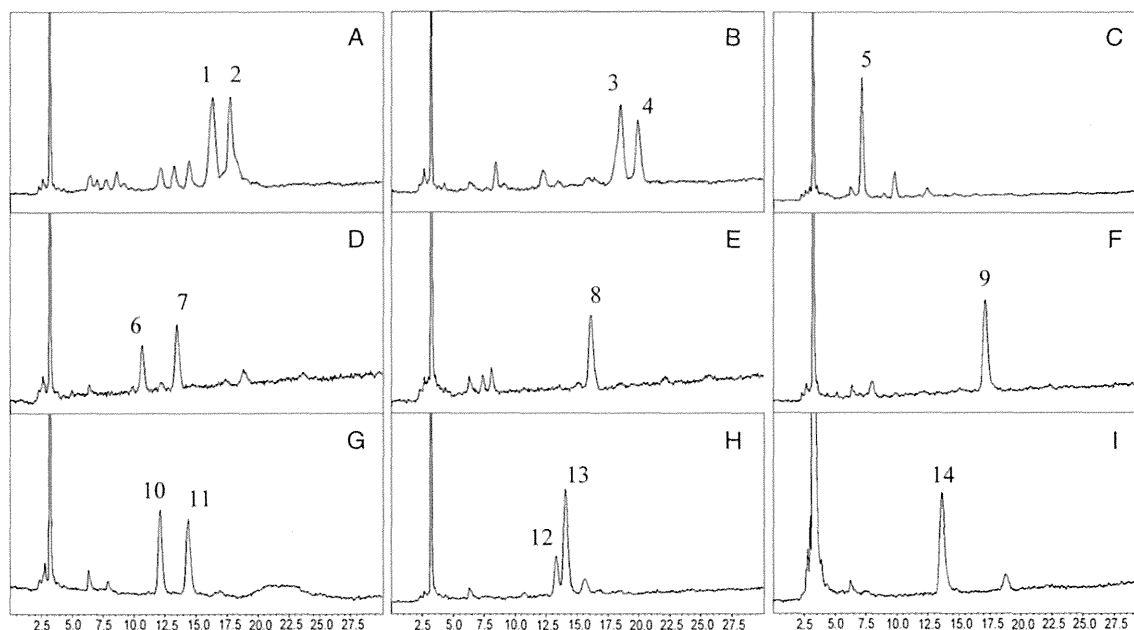
Fig. 4. Amide column elution profiles of PA-glycans from each fraction separated on the ODS column of human islets. (A) ODS peak-N5. Peaks 1 and 2 correspond to N5-1 and N5-2, respectively. (B) ODS peak-N6. Peaks 3 and 4 correspond to N6-1 and N6-2, respectively. (C) ODS peak-N11. Peak 5 corresponds to N11. (D) ODS peak-N12. Peaks 6 and 7 correspond to N12-1 and N12-2, respectively. (E) ODS peak-N13. Peak 8 corresponds to N13. (F) ODS peak-M1. Peak 9 corresponds to M1. (G) ODS peak-M2. Peaks 10 and 11 correspond to M2-1 and M2-2, respectively. (H) ODS peak-M4. Peaks 12 and 13 correspond to M4-1 and M4-2, respectively. (I) ODS peak-D2. Peak 14 corresponds to D2.

No terminal fucose was detected in the N-glycans from either type of islets in this study.

Previous studies reported by other groups concluded that many kinds of N-glycans are found in API, using MALDI-TOF/MS and MS/MS (Kim, Gil et al. 2008; Kim, Gil et al. 2009; Kim, Harvey et al. 2009). The difference in the number of detected N-glycans in this study can be attributed to the sensitivity of the MS method and HPLC. It, thus, appears that the accuracy of the data presented here using HPLC mapping in conjunction with a MALDI-TOF technique provided much more detailed information. That is, MS data are sensitive and can be rapidly obtained, but indicate only a glycan structure based on the calculated molecular weight. Therefore, discriminating between isomeric structures becomes difficult (Wheeler and Harvey 2001). In addition, except for N-glycolylneuraminic acid (NeuGc), it does not indicate the specific structure of sialyl acids present. On the other hand, the data reported herein can be used to identify the representative features of each N-glycan in the API preparation. However, the possibility that several glycans, such as pN6-2, pM2-1, pM2-2, pM3-1, pM3-2 and pM5, that were not detected in humans islets as major N-glycans are expressed in human islets at very low levels cannot be completely excluded. In addition, concerning the sulfated N-glycans such as S1-1, S1-2, S2, MS1 and MS3, the accuracy in identifying the

position of the SOH3 attached to β1-4GalNAc was not clear in this study, and it is possible that these sulfated glycans also may be produced in human islets or other tissues, because humans produce several sulfotransferase enzymes that can catalyze the attachment of a sulfate to GalNAc (Boregowda et al. 2005).

Chlorate is a selective inhibitor of adenosine triphosphate sulfate adenylyltransferase, the first enzyme in the sulfate activation pathway (Girard et al. 1998). It inhibits all sulfotransferases. Therefore, although API had a diminished antigenicity to human serum, especially IgM, as a result of the presence of sodium chlorate treatment, a structural analysis of the changes on the sulfated N-glycans and other nonsulfated glycans of the API after the treatment might be needed to assess antigenicity issues. On the other hand, it was not possible to determine the binding site of the sulfate residue to GalNAc using this method. However, the possibility that the sulfate residue is one of the non-Gal antigens in pig islets cannot be excluded based on the data presented herein. Further study will be needed to analyze the non-Gal antigen in pig islets, especially to sulfotransferase enzymes.

In comparison with a report concerning the pig lung and trachea, using exactly the same HPLC mapping in conjunction with the MALDI-TOF technique, Sriwilaijaroen et al. (2011) reported a relatively small percent of high-mannose type

Peak 16 corresponds to M1. (K) ODS peak-M2. Peaks 17 and 18 correspond to M2-1 and M2-2, respectively. (L) ODS peak-M3. Peaks 19 and 20 correspond to M3-1 and M3-2, respectively. (M) ODS peak-M4. Peak 21 corresponds to M4. N: ODS peak-M5. Peak 22 corresponds to M5. (O) ODS peak-M6. Peak 23 corresponds to M6. (P) ODS peak-S1. Peaks 24 and 25 were identified as S1-1 and S1-2, respectively. (Q): ODS peak-D1. Peak 26 corresponds to D1. (R) ODS peak-D2. Peak 27 corresponds to D2. (S) ODS peak-D3. Peak 28 corresponds to D3. (T) ODS peak-MS1. Peak 29 corresponds to MS1. Peak 30 is the epimerization of ODS peak-MS2. (U) ODS peak-MS2. Peak 31 corresponds to MS2. (V) ODS peak-MS3. Peak 32 corresponds to MS3. (W) ODS peak-S2. Peak 33 corresponds to S2. *Not a sugar.
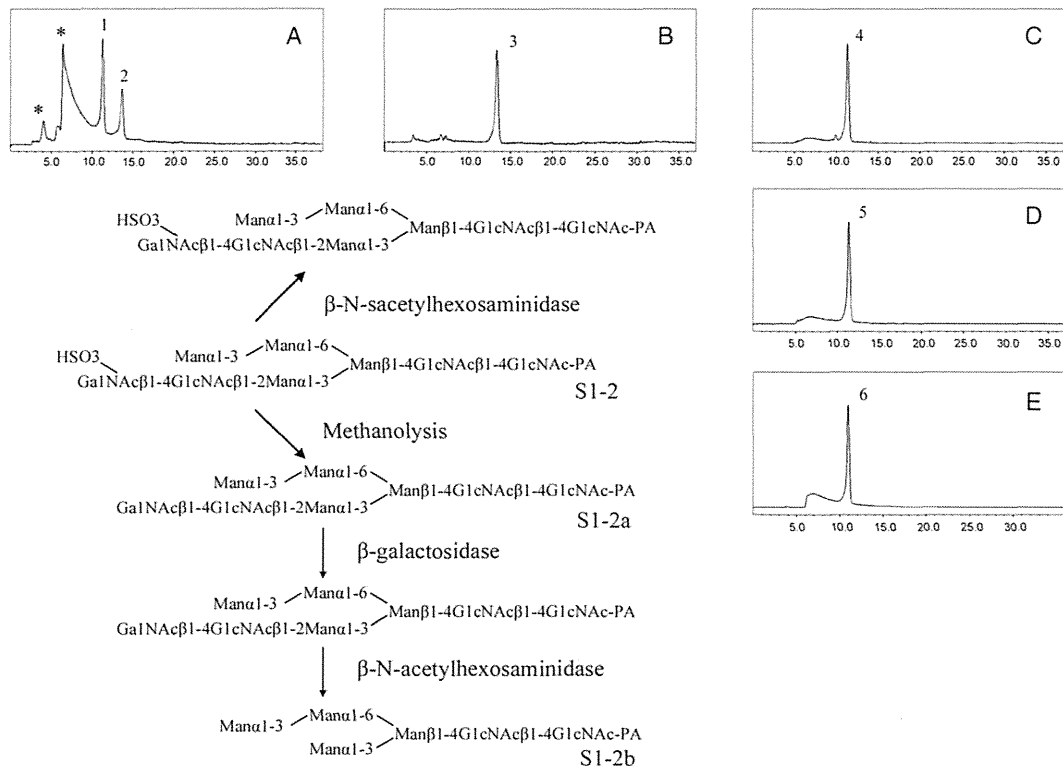
HSO3 Manα1-3 ╱Manα1-6╲
GalNAcβ1-4GlcNAcβ1-2Manα1-3 ╱ Manβ1-4GlcNAcβ1-4GlcNAc-PA

β-N-sacetylhexosaminidase

HSO3 Manα1-3 ╱Manα1-6╲
GalNAcβ1-4GlcNAcβ1-2Manα1-3 ╱ Manβ1-4GlcNAcβ1-4GlcNAc-PA
S1-2

Methanolysis

Manα1-3 ╱Manα1-6╲
GalNAcβ1-4GlcNAcβ1-2Manα1-3 ╱ Manβ1-4GlcNAcβ1-4GlcNAc-PA
S1-2a

β-galactosidase

Manα1-3 ╱Manα1-6╲
GalNAcβ1-4GlcNAcβ1-2Manα1-3 ╱ Manβ1-4GlcNAcβ1-4GlcNAc-PA

β-N-acetylhexosaminidase

Manα1-3 ╱Manα1-6╲
Manα1-3 ╱ Manβ1-4GlcNAcβ1-4GlcNAc-PA
S1-2b

Fig. 5. Structural analysis of S1-2. (**A**) ODS peak after methanolysis treatment of S1-2. Peak 1 is the nonreacted sample, S1-2 (7.5 GU and 1641 Da). Peak 2 corresponds to S1-2a (8.3 GU and 1557 Da). (**B**) ODS peak after β-galactosidase treatment to S1-2a. Peak 3 is identical to S1-2a in ODS (GU) and molecular weight. (**C**) ODS peak after β-N-acetylhexosaminidase treatment of S1-2a. Peak 4 corresponds to S1-2b (7.5 GU and 1151 Da). (**D**) ODS peak after co-chromatography of S1-2b and M4.1. S1-2b was then proved to be the same structure as M4.1 in GALAXY. (**E**) ODS peak after β-galactosidase treatment to S1-2. Peak 6 is just the same as S1-2 in GU and molecular weight. * Not a sugar.

N-glycans. However, in this study, pig islets contain a relatively large percent of N-glycans, 81%, and human islets also contain 76.7%. Therefore, this evidence related to high-mannose types was assumed to be a typical feature of islets. It is noteworthy that in this pig islets study no evidence was found for the presence of α-Gal and NeuGc structures, while the pig lung and trachea clearly produce both antigens. Concerning α-Gal, as has been indicated in many reports, pig islets express very low levels of α-Gal. On the other hand, concerning NeuGc, our previous study reported that NeuGc is expressed on the N-glycans of API (Komoda et al. 2004). Therefore, pig islets must contain NeuGc in relatively minor amounts and, as a result, were not detected in this study, because pig lung and trachea contain relatively minor levels of NeuGc structures.

In addition, NeuGc-Gal-GlcNAc and Galα1-3 Lewis x (Lew[x]) were recently reported as novel antigens, as evidenced by a structural analysis of N-glycans from the miniature pig kidney (Kim et al. 2006). However, neither of these antigens was detected in this study.

Blixt et al. (2009) reported on the carbohydrate specificities of sera obtained from clinical patients in whom neonatal bone pig islet-like cell clusters (NPCC) had been intraportally injected, using a printed covalent glycan array with 200 structurally defined glycans. Besides α-Gal and NeuGc, the patients had Abs against terminal α-linked GalNAc, β3-linked Gal especially Galβ1,3GlcNAc even if terminally sulfated or sialylated, β-GlcNAc except for β1,3-linked, oligomannosyl compounds, some neuranimic acid (NeuAc) and Galα1-3Lew[x]. Compared with the data reported here, pM5 has β-GlcNAc, might be applicable for the target structure of the patients. In addition, N6-2, pM2-2 and pM3-2, which contain Manα1-3Manα1-6Man structures, are also potential target antigens. However, the antigenicity of NPCC may slightly be different from that for API.

As the other non-Gal antigens, the Forssman, the terminal GalNAc related to the Tn-antigen (GalNAcα-O-Ser/Thr), T-antigen (Thomsen-Friedenreich; Galβ3GalNAcα-O-Ser/Thr) and sialyl-Tn antigen (NeuAcα2,6GalNAcα-O-Ser/Thr) are also reported to be important (Ezzelarab et al. 2005). However, these glycans are related to O-glycans and glicolipids (Diswall et al. 2011).

In summary, as a feature, pig islets are rich in high-mannose type N-glycans, especially relatively low amounts of mannose. Several API structures, such as N6-2, pM2-1, 2-2, 3-1, 3-2, and pM5, and the sulfate structure, β-linked GalNAc-SOH3, were not detected in human islets. In addition, it is possible that the sulfated glycans of API are involved in the observed antigenicity to human serum. The data herein provide important information that can be useful to future clinical xenotransplantation studies.
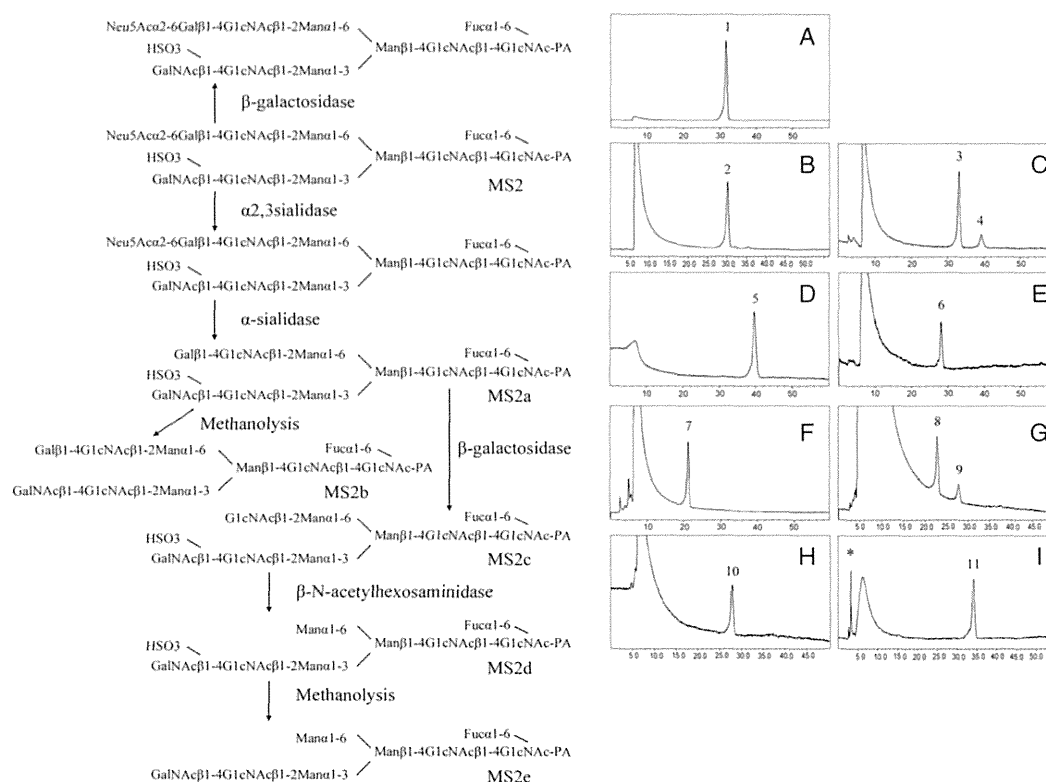
Fig. 6. Structural analysis of MS2. (**A**) ODS peak after α2,3-sialidase treatment to MS2. Peak 1 was just the same as MS2 in GU and molecular weight. (**B**) ODS peak after α-sialidase treatment to MS2. Peak 2 corresponds to MS2a (12.1 GU and 1988 Da). (**C**) ODS peak after methanolysis treatment to MS2a. Peak 3 is the nonreacted sample. Peak 4 lacked one sulfate residue from MS2a and corresponds to MS2b (13.9 GU and 1907 Da). (**D**) ODS peak after co-chromatography of MS2b and 210.4a in GALAXY. MS2b was proved to be the same structure as the 210.4a in GALAXY. (**E**) ODS peak after β-galactisidase treatment to MS2a. Peak 6 lacked one galactose from MS2a and corresponds to MS2c (11.4 GU and 1826 Da). (**F**) ODS peak after β-N-acetylhexosaminidase treatment to MS2c. Peak 7 corresponds to MS2d (9.7 GU and 1622 Da). (**G**) ODS peak after methanolysis treatment of MS2d. Peak 8 was the nonreacted sample. Peak 9 lacked one sulfate residue from MS2d and corresponds to MS2e (11.0 GU and 1541 Da). (**H**) ODS peak after co-chromatography of MS2e and 110.4a in GALAXY. MS2e was proved to be the same structure as the 110.4a in GALAXY. (**I**) ODS peak after β-galactisidase treatment to MS2. Peak 11 is identical to MS2 in GU and molecular weight. * Not a sugar.

Materials and methods

Pig islet isolation

Pancreatic glands were removed from several pigs at a slaughterhouse that handles young market weight pigs (Large White/Landrace x Duroc, 6 months old, ~100 kg). Isolation of porcine islets was performed using the Islet Isolation Technique (Goto et al. 2004), with minor modifications. Purified islet fractions were pooled and cultured at 37°C in a humidified atmosphere with 5% CO_2 in CMRL1066 medium (Biochrom, Berlin, Germany) supplemented with 20% heat inactivated porcine serum, 2 mm N-acetyl-L-alanyl-L-glutamine, 10 mM N-2-hydroxyethylpiperazine-N1-2-ethanesulfonic acid, 100 IU/mL penicillin, 100 µg/mL streptomycin (Biochrom) and 20 µg/mL ciprofloxacin (Bayer, Leverkusen, Germany).

Human islet isolation

The method used to isolate islets has been reported previously (Matsumoto et al. 2002). In brief, the pancreas was distended with a cold enzyme solution through the pancreatic duct using a pressure-controlled pump system. In all cases, the distended pancreata were digested using the semi-automated method (Matsumoto et al. 2006). All centrifuged pellets were collected in cold storage/purification stock solution (Mediatech, Inc., Manassas, VA).

Islet isolations were conducted based on the Edmonton protocol with our modifications. The results of the isolations were evaluated based on the Edmonton protocol. Islets were purified with a COBE 2991 cell processor (CaridianBCT, Inc., Lakewood, CO) using density-adjusted iodixanol-based continuous density gradient. The final preparation of islets was assessed using dithizone staining (Sigma Chemical Co., St. Louis, MO) for islet yield and purity. Islet yield was converted into a standard number of islet equivalents (diameter standardizing to 150 µm). Islet viability was evaluated with fluorescein diacetate (10 µmol/L) and propidium iodide (15 µmol/L) staining. All procedures were done at the Baylor Research Institute, TX.
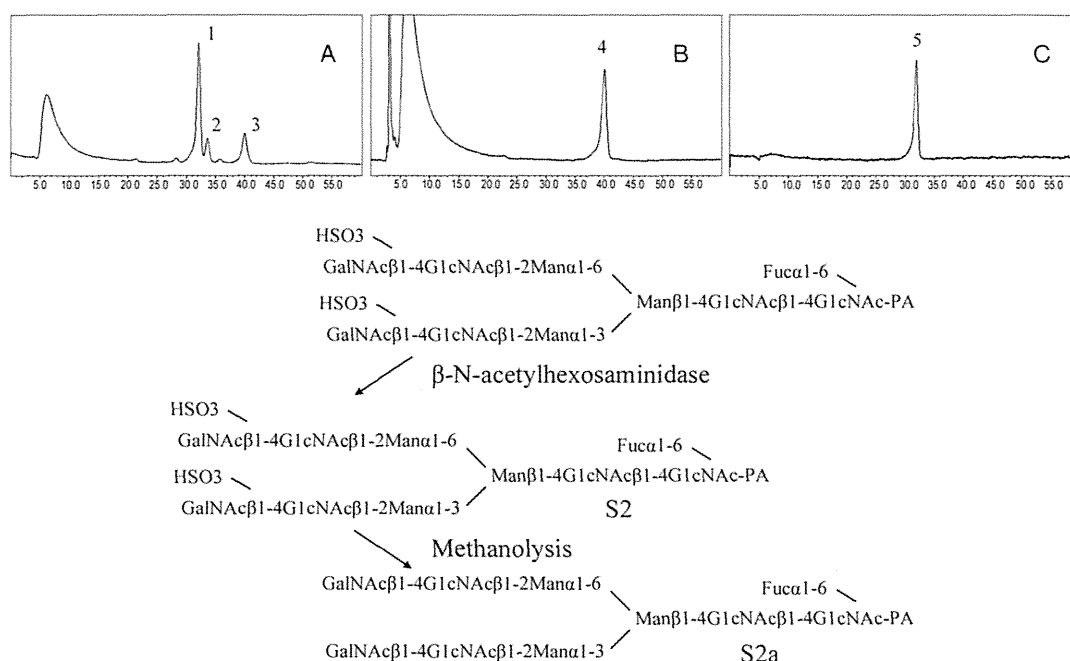
HSO3 ⟍
GalNAcβ1-4GlcNAcβ1-2Manα1-6 ⟍
HSO3 ⟍   Fucα1-6 ⟍
GalNAcβ1-4GlcNAcβ1-2Manα1-3 ╱   Manβ1-4GlcNAcβ1-4GlcNAc-PA

        ╱ β-N-acetylhexosaminidase

HSO3 ⟍
GalNAcβ1-4GlcNAcβ1-2Manα1-6 ⟍
HSO3 ⟍   Fucα1-6 ⟍
GalNAcβ1-4GlcNAcβ1-2Manα1-3 ╱   Manβ1-4GlcNAcβ1-4GlcNAc-PA
                                                      S2

            ⟍ Methanolysis

GalNAcβ1-4GlcNAcβ1-2Manα1-6 ⟍
                                            Fucα1-6 ⟍
                                       Manβ1-4GlcNAcβ1-4GlcNAc-PA
GalNAcβ1-4GlcNAcβ1-2Manα1-3 ╱   S2a

Fig. 7. Structural analysis of S2. (**A**) ODS peak after methanolysis treatment to S2. Peak 1 was the nonreacted sample, S2 (12.7 GU, 2110 Da). Peak 2 lacked one sulfate residue from S2, 13.2 GU and 2029 Da. Peak 2 lacked two sulfate residues from S2, corresponding to S2a (15.1 GU and 1948 Da). (**B**) ODS peak after co-chromatography of the samples of S2a and 210.4b. S2a was the same structure as the 210.4b in GALAXY. (**C**) ODS peak after β-N-acetylhexosaminidase treatment of S2. Peak 5 was identical to S2 in GU and molecular weight.

Materials for analyses

Glycoamidase A from sweet almond, α-manosidase, β-galactosidase and β-N-acetylhexosaminidase from jack bean were purchased from Seikagaku Kogyo Co. (Tokyo, Japan). α-Gal from coffee bean was purchased from Oxford GlycoSciences, Inc. (Oxford, UK). Trypsin and chymotrypsin were obtained from Sigma (St. Louis, MO). Pronase protease from *Streptomyces griseus* was from Calbiochem (San Diego, CA). The PA derivatives of isomalto-oligosaccharides 4–20 (indicating the degree of polymerization of glucose residues) and reference PA-oligosaccharides were purchased from Seikagaku Kogyo Co.

Characterization of N-glycan derived from islets

The residue after extracting each islet with a chloroform–methanol solution was used as the starting material. All experimental procedures used, including the chromatographic conditions and glycosidase treatments, have been described previously (Takahashi et al. 2001). The extract was proteolyzed with chymotrypsin and trypsin mixture and further digested with glycoamidase A to release N-glycans. After the removal of the peptide materials, the reducing ends of the N-glycans were derivatized with 2-aminopyridine (Wako, Osaka, Japan). This mixture was applied to a DEAE column (Tosoh, Tokyo, Japan) or a TSK-gel Amide-80 column (Tosoh), and each fraction that was separated on the amide column was applied to a Shim-pack HRC-ODS column (Shimadzu, Kyoto, Japan). The elution times of the individual peaks onto the amide-silica and ODS columns were normalized with respect to a PA-derivatized isomalto-oligosaccharide with

a known degree of polymerization, and are represented in units of glucose unit (GU). Thus, a given compound from these two columns provided a unique set of GU values, which corresponded to the coordinates of the two dimension HPLC map. The PA-oligosaccharides were identified by comparison with the coordinates of <500 reference PA-oligosaccharides in a homemade web application, GALAXY (http://www.glycoanalysis.info/) (Takahashi and Kato 2003). The calculated HPLC map based on the unit contribution values was used to estimate some high-mannose type PA-oligosaccharides. The PA-oligosaccharides were co-chromatographed with the reference to PA-oligosaccharides on the columns to confirm their identities.
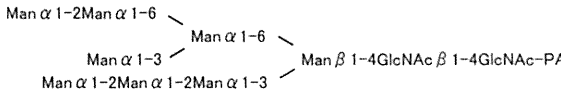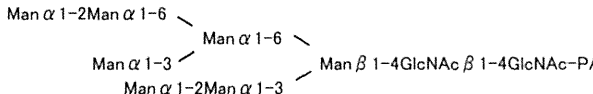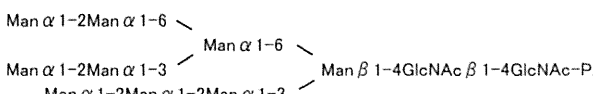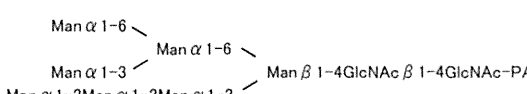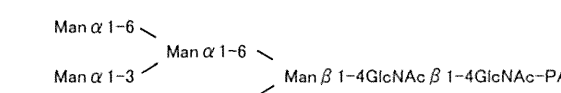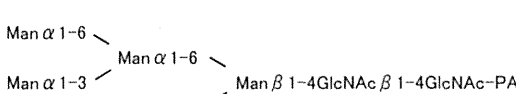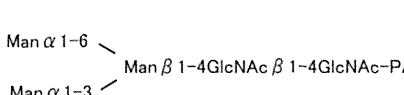
MS analyses of PA-glycans

PA-oligosaccharides were subjected to MALDI-TOF-MS analysis. The matrix solution was prepared as follows: 10 mg of 2,5-dihydroxybenzoic acid (Sigma) was dissolved in 1:1 (v/v) of acetonitrile/water (1 mL). Stock solutions of PA-glycans were prepared by dissolving them in pure water. One microliter of sample solution was mixed on the target spot of a plate with 1 μL of matrix solution and then allowed to air-dry. MALDI-TOF-MS data were acquired in the positive modes using AXIMA-CFR (Shimadzu) operated in the linear mode.

Single islet cell preparation

Single-cell suspensions were prepared by the method described by Ono et al. (1977). Isolated islets were exposed to 0.04% ethylenediaminetetraacetic acid for 5 min at room temperature

Table I. Structures and relative quantities of neutral, mono-sialyl, di-sialyl or mono-sulfate, mono-sialyl-mono-sulfate and di-sulfate PA-oligosaccharides derived from human and porcine islets

Peak code number	GU[a] ODS (Amid)	Molecular[b] mass (Da)	Structure[c]	Relative quantity (%)[d]	
					Pig
Neutral glycan					
N1	4.9 (8.8)	1800	Man α 1–2Man α 1–6 ⟍ Man α 1–6 ⟍ Man β 1–4GlcNAc β 1–4GlcNAc–PA, Man α 1–3 ╱, Man α 1–2Man α 1–2Man α 1–3 ╱	11.6	24.9
N2-1	5.3 (7.9)	1638	Man α 1–2Man α 1–6 ⟍ Man α 1–6 ⟍ Man β 1–4GlcNAc β 1–4GlcNAc–PA, Man α 1–3 ╱, Man α 1–2Man α 1–3 ╱	5.8	3.5
N2-2	5.3 (9.5)	1962	Man α 1–2Man α 1–6 ⟍ Man α 1–6 ⟍ Man β 1–4GlcNAc β 1–4GlcNAc–PA, Man α 1–2Man α 1–3 ╱, Man α 1–2Man α 1–2Man α 1–3 ╱	7.4	9.5
N3	6.0 (7.9)	1638	Man α 1–6 ⟍ Man α 1–6 ╱ Man β 1–4GlcNAc β 1–4GlcNAc–PA, Man α 1–3 ╱, Man α 1–2Man α 1–2Man α 1–3 ╱	3.0	1.9
N4	6.2 (7.0)	1475	Man α 1–6 ⟍ Man α 1–6 ╱ Man β 1–4GlcNAc β 1–4GlcNAc–PA, Man α 1–3 ╱, Man α 1–2Man α 1–2Man α 1–3 ╱	16.7	10.1
pN5 = hN7	7.3 (6.1)	1313	Man α 1–6 ⟍ Man α 1–6 ⟍ Man β 1–4GlcNAc β 1–4GlcNAc–PA, Man α 1–3 ╱, Man α 1–3 ╱	24.0	11.3
pN6-1 = hN8	7.5 (4.2)	989	Man α 1–6 ⟍ Man β 1–4GlcNAc β 1–4GlcNAc–PA, Man α 1–3 ╱	2.3	6.2

Continued

Table I. (Continued)

Peak code number	GU[a] ODS (Amid)	Molecular[b] mass (Da)	Structure[c]	Relative quantity (%)[d]	
				Pig	
pN6-2	7.5 (5.1)	1151	Man α 1-6 — Man α 1-3 ╱ Man β 1-4GlcNAc β 1-4GlcNAc-PA / Man α 1-3 ╱	1.7	–
pN7 = hN9	7.7 (3.3)	827	Man α 1-6 ╲ Man β 1-4GlcNAc β 1-4GlcNAc-PA	2.4	2.2
pN8 = hN10	10.3 (4.6)	1135	Man α 1-6 ╲ Fuc α 1-6 ╲ Man β 1-4GlcNAc β 1-4GlcNAc-PA / Man α 1-3 ╱	3.9	4.1
pN9 = hN11	10.5 (3.7)	973	Man α 1-6 ╲ Fuc α 1-6 ╲ Man β 1-4GlcNAc β 1-4GlcNAc-PA	2.2	3.0
hN12-1	12.8 (5.4)	1541	GlcNAc β 1-2Man α 1-6 ╲ Fuc α 1-6 ╲ Man β 1-4GlcNAc β 1-4GlcNAc-PA / GlcNAc β 1-2Man α 1-3 ╱	–	1.8
hN12-2	12.8 (6.5)	1948	Gal β 1-4GlcNAc β 1-6 ╲ / Man α 1-6 ╲ Fuc α 1-6 ╲ / Gal β 1-4GlcNAc β 1-2 ╱ Man β 1-4GlcNAc β 1-4GlcNAc-PA / Gal β 1-4GlcNAc β 1-4 ╲ / Man α 1-3 ╱ / Gal β 1-4GlcNAc β 1-2 ╱	–	2.9
hN13	14.2 (7.4)	1866	Gal β 1-4GlcNAc β 1-2Man α 1-6 ╲ Fuc α 1-6 ╲ Man β 1-4GlcNAc β 1-4GlcNAc-PA / Gal β 1-4GlcNAc β 1-2Man α 1-3 ╱	–	3.1
hN5-1	6.6 (7.4)	1558	(Hexose)4(HexNAc)4(PA)1[e]	–	2.7
hN5-2	6.6 (7.9)	1720	(Hexose)5(HexNAc)4(PA)1[e]	–	2.0
hN6-1	6.9 (8.1)	1720	(Hexose)5(HexNAc)4(PA)1[e]	–	1.5
hN6-2	6.9 (8.5)	1882	(Hexose)6(HexNAc)4(PA)1[e]	–	1.2

[a]Units of GU were calculated from the elution times of the peaks obtained from the ODS column in Figure 2 and the Amide column in Figure 3.
[b]Average mass calculated from the m/z values of $[M + Na]^+$ or $[M + H]^+$ion for neural, $[M − H]^-$ ion for mono-sialyl and mono-sulfated and $[M + Na − 2H]^-$ ions for mono-sialyl-mono-sulfated and di-sulfated PA-oligosaccharides (Supplementary data, Figure S1).
[c]Structures of PA-oligosaccharides are represented.
[d]Molecular percentage of was calculated from the peak area in Figure 2 by comparison with total N-glycan content in each islet tissue.
[e]N-glycans did not coincide with those of known references in the GALAXY database.

Table II. Structures and relative quantities of neutral, mono-sialyl, di-sialyl or mono-sulfate, mono-sialyl-mono-sulfate and di-sulfate PA-oligosaccharides derived from human and porcine islets

Peak code number	GU[a] ODS (Amid)	Molecular[b] mass (Da)	Structure[c]	Relative quantity (%)[d]	
				Pig	Human
Mono-sialyl glycan					
pM2-1	9.0 (5.4)	1646	Man α 1–6⟍ Man β 1–4GlcNAc β 1–4GlcNAc–PA / Neu5Ac α 2–3Gal β 1–4GlcNAc β 1–2Man α 1–3	0.2	–
pM3-1	11.9 (5.9)	1792	Man α 1–6⟍ Fuc α 1–6 ⟍ Man β 1–4GlcNAc β 1–4GlcNAc–PA / Neu5Ac α 2–3Gal β 1–4GlcNAc β 1–2Man α 1–3	0.3	–
hM2-1	7.9 (6.0)	1646	Man α 1–6⟍ Man β 1–4GlcNAc β 1–4GlcNAc–PA / Neu5Ac α 2–6Gal β 1–4GlcNAc β 1–2Man α 1–3	–	0.15
pM1 = hM3	8.6 (7.1)	1970	Man α 1–6 ⟍ Man α 1–6 ⟍ Man α 1–3 / Man β 1–4GlcNAc β 1–4GlcNAc–PA / Neu5Ac α 2–3Gal β 1–4GlcNAc β 1–2Man α 1–3	0.6	0.2
pM2-2	9.0 (6.2)	1808	Man α 1–6 ⟍ Man α 1–3 / Man β 1–4GlcNAc β 1–4GlcNAc–PA / Neu5Ac α 2–3Gal β 1–4GlcNAc β 1–2Man α 1–3	0.3	–
pM3-2	11.9 (6.7)	1954	Man α 1–6 ⟍ Fuc α 1–6 ⟍ Man α 1–3 / Man β 1–4GlcNAc β 1–4GlcNAc–PA / Neu5Ac α 2–3Gal β 1–4GlcNAc β 1–2Man α 1–3	0.3	–
hM1	7.6 (7.7)	1970	(Hexose)6(HexNAc)3(NEuAc)1(PA)1[e]	–	0.2
hM2-2	7.9 (6.8)	2255	(Hexose)4(HexNAc)6(NeuAc)1(PA)1[e]	–	0.15
hM4-1	11.2 (6.4)	1792	Man α 1–6⟍ Fuc α 1–6 ⟍ Man β 1–4GlcNAc β 1–4GlcNAc–PA / Neu5Ac α 2–6Gal β 1–4GlcNAc β 1–2Man α 1–3	–	0.1
hM4-2	11.2 (6.7)	2011	Gal β 1–4GlcNAc β 1–2Man α 1–6 ⟍ Man β 1–4GlcNAc β 1–4GlcNAc–PA / Neu5Ac α 2–3Gal β 1–4GlcNAc β 1–2Man α 1–3	–	0.4
pM4 = hM5	13.5 (7.6)	2157	Gal β 1–4GlcNAc β 1–2Man α 1–6 ⟍ Fuc α 1–6 ⟍ Man β 1–4GlcNAc β 1–4GlcNAc–PA / Neu5Ac α 2–6Gal β 1–4GlcNAc β 1–2Man α 1–3	0.5	0.5
pM5	14.4 (6.2)	1995	GlcNAc β 1–2Man α 1–6 ⟍ Fuc α 1–6 ⟍ Man β 1–4GlcNAc β 1–4GlcNAc–PA / Neu5Ac α 2–3Gal β 1–4GlcNAc β 1–2Man α 1–3	0.6	–
M6	15.1 (7.1)	2157	Gal β 1–4GlcNAc β 1–2Man α 1–6 ⟍ Fuc α 1–6 ⟍ Man β 1–4GlcNAc β 1–4GlcNAc–PA / Neu5Ac α 2–3Gal β 1–4GlcNAc β 1–2Man α 1–3	0.6	2.1

[a]Units of GU were calculated from the elution times of the peaks obtained from the ODS column in Figure 2 and the Amide column in Figure 3.
[b]Average mass calculated from the m/z values of $[M + Na]^+$ or $[M + H]^+$ ion for neural, $[M - H]^-$ ion for mono-sialyl and mono-sulfated and $[M + Na - 2H]^-$ ions for mono-sialyl-mono-sulfated and di-sulfated PA-oligosaccharides (Supplementary data, Figure S1).
[c]Structures of PA-oligosaccharides are represented.
[d]Molecular percentage of was calculated from the peak area in Figure 2 by comparison with total N-glycan content in each islet tissue.
[e]N-glycans did not coincide with those of known references in the GALAXY database.

Table III. Structures and relative quantities of neutral, mono-sialyl, di-sialyl or mono-sulfate, mono-sialyl-mono-sulfate and di-sulfate PA-oligosaccharides derived from human and porcine islets

Peak code number	GU[a] ODS (Amid)	Molecular[b] mass (Da)	Structure[c]	Relative quantity (%)[d]	
				Pig	Human
Di-sialyl glycan					
D1	10.6 (7.5)	2302	Neu5Ac α2-6Gal β1-4GlcNAc β1-2Man α1-6 ＼ Man β1-4GlcNAc β1-4GlcNAc-PA; Neu5Ac α2-6Gal β1-4GlcNAc β1-2Man α1-3 ／	0.2	0.4
hD2	12.1 (6.5)	2302	Neu5Ac α2-3Gal β1-4GlcNAc β1-2Man α1-6 ＼ Man β1-4GlcNAc β1-4GlcNAc-PA; Neu5Ac α2-3Gal β1-4GlcNAc β1-2Man α1-3 ／	–	0.3
pD2 = hD3	13.5 (7.9)	2448	Neu5Ac α2-6Gal β1-4GlcNAc β1-2Man α1-6 ＼ Fuc α1-6 ＼ Man β1-4GlcNAc β1-4GlcNAc-PA; Neu5Ac α2-6Gal β1-4GlcNAc β1-2Man α1-3 ／	0.8	0.2
pD3 = hD4	15.8 (6.9)	2448	Neu5Ac α2-3Gal β1-4GlcNAc β1-2Man α1-6 ＼ Fuc α1-6 ＼ Man β1-4GlcNAc β1-4GlcNAc-PA; Neu5Ac α2-3Gal β1-4GlcNAc β1-2Man α1-3 ／	0.5	0.9

[a]Units of GU were calculated from the elution times of the peaks obtained from the ODS column in Figure 2 and the Amide column in Figure 3.
[b]Average mass calculated from the m/z values of [M + Na]⁺ or [M + H]⁺ ion for neural, [M − H]⁻ ion for mono-sialyl and mono-sulfated and [M + Na-2H]⁻ ions for mono-sialyl-mono-sulfated and di-sulfated PA-oligosaccharides (Supplementary data, Figure S1).
[c]Structures of PA-oligosaccharides are represented.
[d]Molecular percentage of was calculated from the peak area in Figure 2 by comparison with total N-glycan content in each islet tissue.
[e]N-glycans did not coincide with those of known references in the GALAXY database.

Table IV. Structures and relative quantities of neutral, mono-sialyl, di-sialyl or mono-sulfate, mono-sialyl-mono-sulfate and di-sulfate PA-oligosaccharides derived from human and porcine islets

Peak code number	GU[a] ODS (Amid)	Molecular[b] mass (Da)	Structure[c]	Relative quantity (%)[d]	
				Pig	Human
Mono-sulfated glycan					
S1-1	7.3 (3.8)	1478	(Hexose)3(HexNAc)4(HSO3)1(PA)1[e]	0.2	–
S1-2	7.3 (4.5)	1641	Man α1-6 ＼; SHO3 ＼ Man α1-3 ／ Man β1-4GlcNAc β1-4GlcNAc-PA; GalNAc β1-4GlcNAc β1-2Man α1-3 ／	0.6	–

[a]Units of GU were calculated from the elution times of the peaks obtained from the ODS column in Figure 2 and the Amide column in Figure 3.
[b]Average mass calculated from the m/z values of [M + Na]⁺ or [M + H]⁺ ion for neural, [M − H]⁻ ion for mono-sialyl and mono-sulfated and [M + Na − 2H]⁻ ions for mono-sialyl-mono-sulfated and di-sulfated PA-oligosaccharides (Supplementary data, Figure S1).
[c]Structures of PA-oligosaccharides are represented.
[d]Molecular percentage of was calculated from the peak area in Figure 2 by comparison with total N-glycan content in each islet tissue.
[e]N-glycans did not coincide with those of known references in the GALAXY database.

and collected by centrifugation at 400 × g for 1 min. The islets were then suspended in 4 mL of 1000 PU/mL Dispase-II (Godo-Shusei Co. Tokyo, Japan) and treated at 37°C for 15 min. Cell aggregates were allowed to settle and the supernatant was transferred to a conical tube. The pooled harvests were centrifuged at 400 × g for 3 min. The cell pellet was washed twice with phosphate buffer saline (PBS) and re-suspended in PBS.

Flowcytometry

The islets were incubated with a 10% solution of normal human pooled serum (NHS) at 4°C for 1 h, washed and then incubated with 1.25 µg of fluorescein isothiocynate-conjugated anti-human IgG and IgM (Cappel, West Chester, PA) as a second antibody for 1 h at 4°C. The stained cells were analyzed with a FACS Calibur flow cytometer (Nippon Becton Dickinson, Tokyo, Japan).

Sulfate-depleted cells

Islets were starved for 24 h in sulfate-free RPMI1640 medium containing 1% of fetal cow serum supplemented with fresh 10 mM sodium chlorate (Nakarai Tesque, Kyoto, Japan).

Supplementary data

Supplementary data for this article are available online at http://glycob.oxfordjournals.org/.

Table V. Structures and relative quantities of neutral, mono-sialyl, di-sialyl or mono-sulfate, mono-sialyl-mono-sulfate and di-sulfate PA-oligosaccharides derived from human and porcine islets

Peak code number	GU[a] ODS (Amid)	Molecular[b] mass (Da)	Structure[c]	Relative quantity (%)[d]	
				Pig	Human
Mono-sialyl-mono-sulfated glycan					
MS1	9.8 (5.0)	2133	(Hexose)4(HexNAc)5(NeuAc)1(HSO3)1(PA)1[e]	0.3	–
MS2	12.7 (5.3)	2279	Neu5Ac α2–6Gal β 1–4GlcNAc β 1–2Man α 1–6 SHO3 GalNAc β 1–4GlcNAc β 1–2Man α 1–3 Fuc α 1–6 Man β 1–4GlcNAc β 1–4GlcNAc–PA	1.3	–
MS3	15.9 (5.4)	2279	(Hexose)4(HexNAc)5(Deoxyhexose)1(NeuAc)1(HSO3)1(PA)1*	0.4	–

[a]Units of GU were calculated from the elution times of the peaks obtained from the ODS column in Figure 2 and the Amide column in Figure 3.
[b]Average mass calculated from the *m/z* values of [M + Na]⁺ or [M + H]⁺ ion for neural, [M − H]⁻ ion for mono-sialyl and mono-sulfated and [M + Na − 2H]⁻ ions for mono-sialyl-mono-sulfated and di-sulfated PA-oligosaccharides (Supplementary data, Figure S1).
[c]Structures of PA-oligosaccharides are represented.
[d]Molecular percentage of was calculated from the peak area in Figure 2 by comparison with total N-glycan content in each islet tissue.
[e]N-glycans did not coincide with those of known references in the GALAXY database.

Table VI. Structures and relative quantities of neutral, mono-sialyl, di-sialyl or mono-sulfate, mono-sialyl-mono-sulfate and di-sulfate PA-oligosaccharides derived from human and porcine islets

Peak code number	GU[a] ODS (Amid)	Molecular[b] mass (Da)	Structure[c]	Relative quantity (%)[d]	
				Pig	Human
Di-sulfated glycan					
S2	12.7 (3.9)	2110	SHO3 GalNAc β 1–4GlcNAc β 1–2Man α 1–6 SHO3 GalNAc β 1–4GlcNAc β 1–2Man α 1–3 Fuc α 1–6 Man β 1–4GlcNAc β 1–4GlcNAc–PA	7.0	–

[a]Units of GU were calculated from the elution times of the peaks obtained from the ODS column in Figure 2 and the Amide column in Figure 3.
[b]Average mass calculated from the *m/z* values of [M + Na]⁺ or [M + H]⁺ ion for neural, [M − H]⁻ ion for mono-sialyl and mono-sulfated and [M + Na − 2H]⁻ ions for mono-sialyl-mono-sulfated and di-sulfated PA-oligosaccharides (Supplementary data, Figure S1).
[c]Structures of PA-oligosaccharides are represented.
[d]Molecular percentage of was calculated from the peak area in Figure 2 by comparison with total N-glycan content in each islet tissue.
[e]N-glycans did not coincide with those of known references in the GALAXY database.
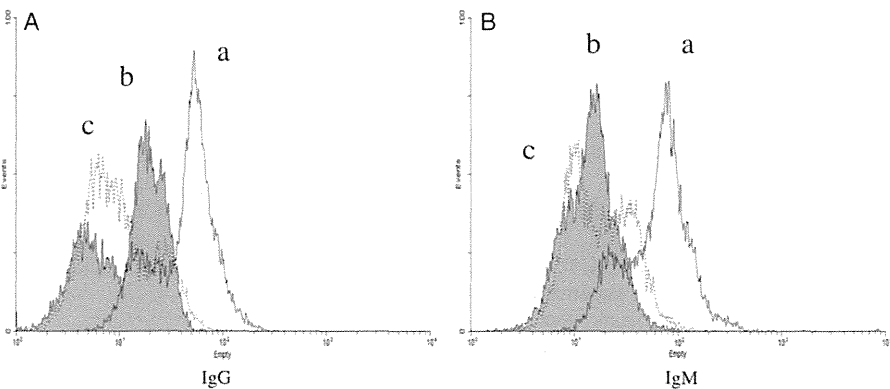

Fig. 8. FACS analysis for the antigenicity of sulfate structures. Islets from adult pigs were treated with 10% NHS as the first antibody and anti-human immmunoglobulins as the second antibodies. Typical FACS profiles of human IgG (**A**) and IgM (**B**) deposition on islets are shown. The effect of removal of sulfate structures by sodium chlorate and sulfate-free medium on the antigenicity of pig islet cells was next investigated. The presence of sodium chlorate led to a reduction in the reactivity of islets to a natural antibody, suggesting that the sulfate structures of islets contain a considerable amount of natural antibody epitopes; a, Normal line: API in usual medium; b, painted out: Sulfate depleted API and c, dotted line: Second antibody control.

Funding

Acknowledgements

Conflict of interest

None declared.

Abbreviations

2D, two dimension; API, adult pig islets; ATP, adenosine triphosphate; DEAE, diethylaminoethyl; FCS, fetal cow serum; FITC, fluorescein isothiocynate; GALAXY, glycoanalysis by the three axes of MS and chromatography; GalNAc, N-acetylgalactosamine; GKO, α1-3-galactosyltransferase knockout; GlcNAc, N-acetylglucosamine; GU, glucose unit; Hex, hexose; HexNAc, N-acetylhexosamine; HPLC, high-performance liquid chromatography; Lew^x, Lewis x; MALDI-TOF-MS, matrix-assisted laser desorption/ionization time-of-flight mass spectrometric; Man, mannose; MS2, mono-sialyl-mono-sulfate; NeuAc, neuranimic acid; NeuGc, N-glycolylneuraminic acid; NHS, normal human pooled serum; ODS, octa decyl silyl; PA, pyridylamino; PBS, phosphate buffer saline; S2, di-sulfate; α-Gal, α-galactosidase.

References

Blixt O, Kumagai-Braesch M, Tibel A, Groth CG, Holgersson J. 2009. Anticarbohydrate antibody repertories in patients transplanted with fetal pig islets revealed by glycan arrays. *Am J Transplant.* 9:83–90.

Boregowda RK, Mi Y, Bu H, Baenziger JU. 2005. Differential expression and enzymatic properties of GalNAc-4-sulfotransferase-1 and GalNAc-4-sulfotransferase-2. *Glycobiology.* 15:1349–1358.

Breimer ME. 2011. Gal/non-Gal antigens in pig tissues and human non-Gal antibodies in the GalT-KO era. *Xenotransplantation.* 18:215–228.

Byrne GW, Stalboerger PG, Du Z, Davis TR, McGregor CG. 2011. Identification of new carbohydrate and membrane protein antigens in cardiac xenotransplantation. *Transplantation.* 91:287–292.

Dai Y, Vaught TD, Boone J, Chen SH, Phelps CJ, Ball S, Monahan JA, Jobst PM, McCreath KJ, Lamborn AE, et al. 2002. Targeted disruption of the alpha1,3-galactosyltransferase gene in cloned pigs. *Nat Biotechnol.* 20:251–255.

Diswall M, Gustafsson A, Holgersson J, Sandrin MS, Breimer ME. 2011. Antigen-binding specificity of anti-αGal reagents determined by solid-phase glycolipid-binding assays. A complete lack of αGal glycolipid reactivity in α1,3GalT-KO pig small intestine. *Xenotransplantation.* 18:28–39.

Elliott RB. 2011. Towards xenotransplantation of pig islets in the clinic. *Curr Opin Organ Transplant.* 16:195–200.

Ezzelarab M, Ayares D, Cooper DK. 2005. Carbohydrates in xenotransplantation. *Immunol Cell Biol.* 83:396–404.

Galili U, Clark MR, Shohet SB, Buehler J, Macher BA. 1987. Evolutionary relationship between the natural anti-Gal antibody and the Gal alpha 1—3Gal epitope in primates. *Proc Natl Acad Sci USA.* 84:1369–1373.

Girard JP, Baekkevold ES, Amalric F. 1998. Sulfation in high endothelial venules:cloning and expression of the human PAPS synthetase. *FASEB J.* 12:603–612.

Goto M, Eich TM, Felldin M, Foss A, Källen R, Salmela K, Tibell A, Tufveson G, Fujimori K, Engkvist M, et al. 2004. Refinement of the automated method for human islet isolation and presentation of a closed system for in vitro islet culture. *Transplantation.* 78:1367–1375.

Kim YG, Gil GC, Harvey DJ, Kim BG. 2008. Structural analysis of alpha-Gal and new non-Gal carbohydrate epitopes from specific pathogen-free miniature pig kidney. *Proteomics.* 8:2596–2610.

Kim YG, Gil GC, Jang KS, Lee S, Kim HI, Kim JS, Chung J, Park CG, Harvey DJ, Kim BG. 2009. Qualitative and quantitative comparison of N-glycans between pig endothelial and islet cells by high-performance liquid chromatography and mass spectrometry-based strategy. *J Mass Spectrom.* 44:1087–1104.

Kim YG, Harvey DJ, Yang YH, Park CG, Kim BG. 2009. Mass spectrometric analysis of the glycosphingolipid-derived glycans from miniature pig endothelial cells and islets: Identification of NeuGc epitope in pig islets. *J Mass Spectrom.* 44:1489–1499.

Kim YG, Kim SY, Hur YM, Joo HS, Chung J, Lee DS, Royle L, Rudd PM, Dwek RA, Harvey DJ, et al. 2006. The identification and characterization of xenoantigenic nonhuman carbohydrate sequences in membrane proteins from porcine kidney. *Proteomics.* 6:1133–1142.

Komoda H, Miyagawa S, Kubo T, Kitano E, Kitamura H, Omori T, Ito T, Matsuda H, Shirakura R. 2004. A study of the xenoantigenicity of adult pig islets cells. *Xenotransplantation.* 11:237–246.

Matsumoto S, Okitsu T, Iwanaga Y, Noguchi H, Nagata H, Yonekawa Y, Yamada Y, Fukuda K, Shibata T, Kasai Y, et al. 2006. Successful islet transplantation from nonheartbeating donor pancreata using modified Ricordi islet isolation method. *Transplantation.* 82:460–465.

Matsumoto S, Qualley SA, Goel S, Hagman DK, Sweet IR, Poitout V, Strong DM, Robertson RP, Reems JA. 2002. Effect of the two-layer (University of Wisconsin solution-perfluorochemical plus O$_2$) method of pancreas preservation method on human islet isolation, as assessed by the Edmonton isolation protocol. *Transplantation.* 74:1414–1419.

Miyagawa S, Ueno T, Nagashima H, Takama Y, Fukuzawa M. 2012. Carbohydrate antigens. *Curr Opin Organ Transplant.* 17:174–179.

Ono J, Takaki R, Fukuma M. 1977. Preparation of single cells from pancreatic islets of adult rat by the use of dispase. *Endocrinol Jpn.* 24:265–270.

Sriwilaijaroen N, Kondo S, Yagi H, Takemae N, Saito T, Hiramatsu H, Kato K, Suzuki Y. 2011. N-glycans from porcine trachea and lung: Predominant NeuAcα2–6Gal could be a selective pressure for influenza variants in favor of human-type receptor. *PLoS One.* 6:e16302.

Takahagi Y, Fujimura T, Miyagawa S, Nagashima H, Shigehisa T, Shirakura R, Murakami H. 2005. Production of alpha 1,3-galactosyltransferase gene knockout pigs expressing both human decay-accelerating factor and N-acetylglucosaminyltransferase III. *Mol Reprod Dev.* 71:331–338.

Takahashi N, Kato K. 2003. GALAXY(Glycoanalysis by the three axes of MS and chromatography): A web application that assists structural analyses of N-glycans. *Trends Glycosci Glycotech.* 15:235–251.

Takahashi N, Khoo KH, Suzuki N, Johnson JR, Lee YC. 2001. N-glycan structures from the major glycoproteins of pigeon egg white: Predominance of terminal Galα(1–4)Gal. *J Biol Chem.* 276:23230–23239.

Thompson P, Badell IR, Lowe M, Cano J, Song M, Leopardi F, Avila J, Ruhil R, Strobert E, Korbutt G, et al. 2011. Islet xenotransplantation using gal-deficient neonatal donors improves engraftment and function. *Am J Transplant.* 11:2593–2602.

Varki A. 2009. Multiple changes in sialic acid biology during human evolution. *Glycoconj J.* 26:231–245.

Wheeler SF, Harvey DJ. 2001. Extension of the in-gel release method for structural analysis of neutral and sialylated N-linked glycans to the analysis of sulfated glycans:application to the glycans from bovine thyroid-stimulating hormone. *Anal Biochem.* 296:92–100.

Yagi H, Takahashi N, Yamaguchi Y, Kimura N, Uchimura K, Kannagi R, Kato K. 2005. Development of structural analysis of sulfated N-glycans by multidimensional high performance liquid chromatography mapping methods. *Glycobiology.* 15:1051–1060.

Yamamoto A, Ikeda K, Wang D, Nakatsu S, Takama Y, Ueno T, Nagashima H, Kondo A, Fukuzawa M, Miyagawa S. 2013. Trial using pig cells with the H-D antigen knocked down. *Surg Today.* 43:782–786.

Satoshi Nishimura,[1,2,3] Mika Nagasaki,[1,4] Shinichi Okudaira,[5] Junken Aoki,[5] Tsukasa Ohmori,[3]
Ryunosuke Ohkawa,[6] Kazuhiro Nakamura,[6] Koji Igarashi,[7] Hiroshi Yamashita,[1] Koji Eto,[8] Kansei Uno,[1,4]
Naoto Hayashi,[4] Takashi Kadowaki,[2,9] Issei Komuro,[1] Yutaka Yatomi,[6] and Ryozo Nagai[3]

CrossMark

ENPP2 Contributes to Adipose Tissue Expansion and Insulin Resistance in Diet-Induced Obesity

OBESITY STUDIES

Body weight is tightly regulated by food intake and energy dissipation, and obesity is related to decreased energy expenditure (EE). Herein, we show that nucleotide pyrophosphatase/phosphodiesterase 2 (ENPP2, autotaxin) is an adipose-derived, secreted enzyme that controls adipose expansion, brown adipose tissue (BAT) function, and EE. In mice, Enpp2 was highly expressed in visceral white adipose tissue and BAT and is downregulated in hypertrophied adipocytes/adipose tissue. Enpp2+/− mice and adipocyte-specific Enpp2 knockout mice fed a high-fat diet showed smaller body weight gains and less insulin resistance than control mice fed the same diet. BAT was functionally more active and EE was increased in Enpp2-deficient mice. In humans, ENPP2 expression in subcutaneous fat and ENPP2 levels in serum were reduced in obese subjects. Taken together, our results establish ENPP2 as an adipose-derived, secreted enzyme that regulates adipose obesity and systemic metabolism. They also suggest ENPP2 could be a useful therapeutic target for the treatment of metabolic disease.

Until recently, adipose tissue was viewed as a passive energy storage organ, but with the discovery of leptin and the adipose-derived humoral factors now known as "adipokines," it has become apparent that adipose tissue is an active endocrine organ that is essential for energy homeostasis (1). Moreover, obese adipose tissue secretes various inflammatory cytokines, including interleukin-6 (IL-6) and tumor necrosis factor-α (TNF-α), whose activities are known to contribute to the development of metabolic and cardiovascular diseases (2).

Enpp2, also designated autotaxin, phosphodiesterase I α/autotaxin, and nucleotide pyrophosphatase/phosphodiesterase 2, was originally discovered as an autocrine motility-stimulating factor released from cancer cells (3). ENPP2 catalyzes the conversion of lysophosphatidylcholine to lysophosphatidic acid (LPA), which exerts a variety of biological effects, in part via G-protein–coupled receptors (3,4). In addition, the COOH-terminal noncatalytic domain of ENPP2 also has biological effects independent of LPA (3). Homozygous Enpp2-deficient mice die in utero due to profound vascular defects, but heterozygous Enpp2-deficient (Enpp2+/−) mice are apparently healthy, with plasma LPA levels about half those in wild-type (WT) mice (5). Enpp2 is reportedly expressed in mouse adipose tissue and 3T3-F442A preadipocytes, and medium conditioned by Enpp2-expressing COS7 cells increased proliferation of 3T3-F442A cells. Recently, Dusaulcy et al. (6) reported that adipocyte-specific Enpp2 knockout (KO) mice fed a high-fat diet showed greater adiposity and less systemic insulin resistance

[1]Department of Cardiovascular Medicine, University of Tokyo, Tokyo, Japan
[2]Translational Systems Biology and Medicine Initiative, University of Tokyo, Tokyo, Japan
[3]Research Division of Cell and Molecular Medicine, Center for Molecular Medicine, Jichi Medical University, Tochigi, Japan
[4]Computational Diagnostic Radiology and Preventive Medicine, University of Tokyo, Tokyo, Japan
[5]Department of Molecular and Cellular Biochemistry, Graduate School of Pharmaceutical Sciences, Tohoku University, Miygai, Japan
[6]Department of Clinical Laboratory, University of Tokyo Hospital, Tokyo, Japan
[7]Bioscience Division, Reagent Development Department, AIA Research Group, Tosoh Corporation, Kanagawa, Japan

[8]Center for iPS Cell Research and Application, Kyoto University, Kyoto, Japan
[9]Department of Metabolic Diseases, University of Tokyo, Tokyo, Japan

Corresponding author: Satoshi Nishimura, snishi-tky@umin.ac.jp.

Received 5 November 2013 and accepted 23 June 2014.

This article contains Supplementary Data online at http://diabetes.diabetesjournals.org/lookup/suppl/doi:10.2337/db13-1694/-/DC1.

S.N. and M.N. contributed equally to this work.

than control mice, with no difference in food intake. By contrast, Federico et al. (7) reported that fat pad weights were higher in mice overexpressing *Enpp2*, although locomotor activities, thermogenic profiles, and systemic metabolism were unchanged. These apparently contradictory results prompted us to examine the role of *Enpp2* in systemic metabolism. Our findings demonstrate that ENPP2 is a key regulator of brown adipose tissue (BAT) function, energy expenditure (EE), and adipose tissue expansion associated with obesity and metabolic conditions.

RESEARCH DESIGN AND METHODS

Animal Models

$Enpp2^{+/-}$ mice were provided by Shinichi Okudaira and Junken Aoki (Department of Molecular and Cellular Biochemistry, Graduate School of Pharmaceutical Sciences, Tohoku University, Miyagi, Japan) (8). Adipocyte-specific (Fat) *Enpp2* KO mice were generated as previously reported (6). $Enpp2^{F/F}$ mice carrying a conditional *Enpp2*-deleted allele (encoding for the catalytic site of *Enpp2*) flanked by two loxP sites were crossed with *Fabp4*-Cre mice (obtained from The Jackson Laboratory). $Enpp2^{F/F}$ *Fabp4*-Cre (Fat-*Enpp2* KO) mice were compared with control $Enpp2^{F/F}$ littermates of the same generation.

Mice selectively overexpressing ENPP2 in their adipocytes were generated as follows. A 5.5-kb cDNA fragment corresponding to positions −5.4k to +62 of the murine *Fabp4* (*aP2*) promoter was ligated to a 2.5-kb fragment corresponding to positions +1 to +2,475 of Enpp2 (NM_001136077), which included a bovine growth hormone polyadenylation signal. The linearized 9.6-kb MluI-KasI FABP4-ENPP2 construct was injected into pronuclei of fertilized zygotes from C57BL/6 mice and transferred to pseudopregnant females. Offspring were then screened for genomic integration by PCR, and mice were generated by breeding F1 heterozygous transgenic males to WT females.

The background of all the mice was C57BL/6J. Littermates for $Enpp2^{+/-}$ (shown as $Enpp2^{+/+}$) were also used as controls. All mice were housed under a 12-h light-dark cycle and allowed free access to food.

To examine the changes in metabolic phenotype seen in diet-induced obesity, we divided C57BL/6 mice into two groups and then fed one group a standard chow diet (6% fat; Oriental Yeast Co., Ltd.) and the other a high-fat diet (D12492, 60 kcal % fat; Research Diets) for 10 weeks, beginning when the mice were 7 weeks old. We performed glucose tolerance tests (oral, 1 g/kg, after 16 h of fasting) at age 14 and 17 weeks and insulin tolerance tests (i.p., 1 unit/kg, after 3.5 h of fasting) at 16 weeks to assess glucose intolerance and insulin resistance. Exercise activity, oxygen consumption, and carbon dioxide production were measured using an Oxymax system (Columbus Instruments).

Interscapular BAT was also surgically removed under microscopic observation for analysis. We were able to differentiate BAT from white adipose tissue (WAT) based on its color and confirmed this identification by histological analysis.

Interstitial fluid was sampled from epididymal fat pad using a modification of an earlier method (9). After placing microdialysis catheters inside the epididymal fat pads of anesthetized mice, saline was injected from the catheters at a rate of 2 μL/min. The interstitial fluid was then sampled 60 min after implantation of the catheters.

The body temperatures of the mice were measured using an electronic thermistor equipped with a rectal probe while the mice were exposed to room temperature and 4°C. Body core temperature was measured at selected times up to 3 h.

All experiments were approved by the ethics committee for animal experiments of the University of Tokyo and Jichi Medical University, and strictly adhered to the guidelines for animal experiments.

Collagenase Digestion

We isolated stromal vascular (SV) cells using previously described methods (10,11) with some modification. Mice were killed under general anesthesia following systemic heparinization. We then removed epididymal, subcutaneous, mesenteric, and BAT and minced them into small pieces, which were incubated for 20 min in collagenase solution (2 mg/mL of collagenase type 2 [Worthington] in Tyrode buffer) with gentle stirring. The digested tissue was then centrifuged, and the resultant pellet containing the SV fraction was resuspended in PBS and filtered through 70-μm mesh. We then washed the collected cells twice with PBS, incubated them for 10 min in erythrocyte-lysing buffer as previously described (12), and finally resuspended them in PBS supplemented with 3% FBS. Isolated adipocytes or SV fractions were further used for imaging, culture, and flow cytometric analysis.

Flow Cytometry of SV Fractions

The isolated cells were labeled with either a monoclonal antibody or an isotype control antibody and analyzed by flow cytometry using a Canto II, Aria (Becton Dickinson), or SP6800 cytometer (Sony), and FlowJo 7.6.5. software (Tomy Digital Biology). We used propidium iodide to exclude dead cells, and adipocyte numbers were determined after collagenase digestion by counting the floating round adipocytes stained with boron-dipyrromethene (BODIPY). Some cells were analyzed after cell sorting using a MoFlo cell sorter (Dako) or Aria cell sorter (Becton Dickinson).

SV Fraction Culture

The SV fraction from epididymal adipose tissue was harvested as described above and cultured until confluent. The cells were cultured in a standard adipogenic mixture containing dexamethasone, isobutylmethylxanthine (IBMX), and insulin (13). To examine their differentiation status, cells were harvested and real-time PCR analysis or histochemical study was carried out.

Isolated Preadipocyte Culture

We isolated Pref1+ CD34+ preadipocytes from epididymal adipose tissue collected from lean 20-week-old C57BL/6 WT, $Enpp2^{+/-}$, Fat-*Enpp2* KO, and adipocyte-specific

Enpp2-overexpressing mice using a MoFlo or Aria cell sorter. Then using flow cytometry, we confirmed that >99.5% of the sorted cells were preadiopocyte cell fractions. Propidium iodide staining was used to exclude dead cells. Some cells were stained with 5 μmol/L CFSE (CellTrace CFSE Cell Proliferation Kit; Invitrogen) for 15 min, after which 2.5 × 10⁴ cells/mL were cultured in DMEM supplemented with 10% FBS plus recombinant murine ENPP2 (10 ng/mL; R&D Systems) and LPA (1 μmol/L; Sigma-Aldrich) for 48 h. Some cells were treated with si-*Enpp2*, si-*CTRL*, and si-*EDG2* for 24 h prior to the incubation period. After incubation, the cultured cells were harvested and analyzed.

Intravital Microscopy

To visualize ectopic fat accumulation, we used in vivo multiphoton microscopy, which is a modification of conventional single photon methods (12). Mice were anesthetized by injection with urethane (1.5 g/kg), after which the skin was removed, and they were secured to the heated stage of an inverted microscope (Eclipse Ti; Nikon, Tokyo, Japan). BODIPY (Invitrogen), fluorescein-labeled isolectin (Vector Laboratories), and Hoechst 33342 (Invitrogen) were injected into the mice to visualize fat accumulations, vessels, and nuclei, respectively. TMRE (tetramethylrhodamine ethyl ester; Invitrogen) dye was used to monitor mitochondrial membrane potential. The tissue was excited at a wavelength of 860 nm using a Ti:Sapphire laser (Vision II; Coherent, Santa Clara, CA), and images were captured using a Nikon A1R MP system equipped with a 40× (N.A. 1.15) water immersion objective lens (Nikon). More than five animals were examined in each group. Images were quantified by observers blinded to the treatment group using NIS-Elements software (Nikon).

Imaging Live Adipose Tissue

To image living adipose tissue ex vivo, we used a previously described method with some modification (14). Adipose tissues were stained with BODIPY (Invitrogen), Hoechst (Invitrogen), and isolectin (Vector Laboratories) (14), after which the cells were imaged using a two-photon microscope (A1R MP; Nikon). This approach enabled us to visualize adipose tissue structure in detail at depths up to >200 μm and to precisely quantify adipocyte cell numbers. Cell diameters and numbers were quantified using NIS-Elements software by observers blinded to the conditions.

Real-Time Quantitative PCR

For real-time PCR, we homogenized adipose tissue in Trizol (Invitrogen), after which total RNA was purified from the homogenates. A TaqMan fluorogenic reverse transcriptase PCR assay was used to determine relative mRNA levels according to the manufacturer's instructions.

Human Subjects

After obtaining informed consent using an institutional review board–approved protocol, we examined serum samples acquired at periodic health checks. This study was conducted according to the principles outlined in the Declaration of Helsinki, and all protocols were approved by the ethics review committee of Tokyo University School of Medicine. We excluded patients diagnosed with a malignancy, liver disease, chronic kidney disease, ischemic heart disease, or type 2 diabetes. In addition to the screening examination, we used a high-throughput ELISA system to assess levels of ENPP2 in serum collected in the morning, after the patients had fasted for at least 6 h (15). Human total and high-molecular-weight adiponectin levels were assessed using an ELISA kit (Sekisui Medical). We also measured the intimal-medial thickness in the carotid arteries as previously reported; the average of the values measured in the right and left carotid arteries was used as the intimal-medial thickness value (16).

We also acquired subcutaneous adipose tissue from healthy female donors undergoing liposuction of the abdomen or thighs (10). After digesting 1-g samples of each specimen using collagenase, the samples were centrifuged to isolate the SV fractions. Total RNA was then isolated using Trizol (Invitrogen), after which relative mRNA levels were determined using real-time PCR. This study was approved by the ethics committee of the University of Tokyo Hospital.

Statistics

The results are expressed as means ± SEM. The statistical significance of differences between two groups was assessed using Student t tests. Differences among three groups were evaluated using ANOVA followed by post hoc Bonferroni tests. Differences among more than three groups were evaluated using Tukey-Kramer tests. Correlations were examined using the Pearson correlation coefficient test. Values of $P < 0.05$ were considered significant. Regression analysis was used to identify independent determinants of ENPP2 and the percentage of the variance that they explained.

RESULTS

ENPP2 Is Produced by Preadipocytes and Adipocytes

To investigate the functions of ENPP2 in metabolism and obesity, we first assessed its expression in mice. We found that ENPP2 is expressed in various mouse tissues, but is particularly high in adipose tissue (Fig. 1A). Moreover, ENPP2 levels were higher in epididymal fat pads than in subcutaneous or brown fat. After separating the adipocyte and SV fractions, we found that levels of *Enpp2* expression were higher in adipocytes than in the SV fraction, as was reported previously (Fig. 1B) (17). Among the cell types present in the SV fraction, Pref1⁺ CD34⁺ preadipocytes expressed higher levels of ENPP2 than CD11b⁺ F4/80⁺ macrophages or CD8⁺ T cells (Fig. 1C). However, because the preadipocyte fraction was relatively small (~5–10%), ENPP2 levels in the whole SV fraction were lower than in the adipocyte fraction. Collectively, these results indicate that preadipocytes and adipocytes are the major cells producing ENPP2 in WAT.
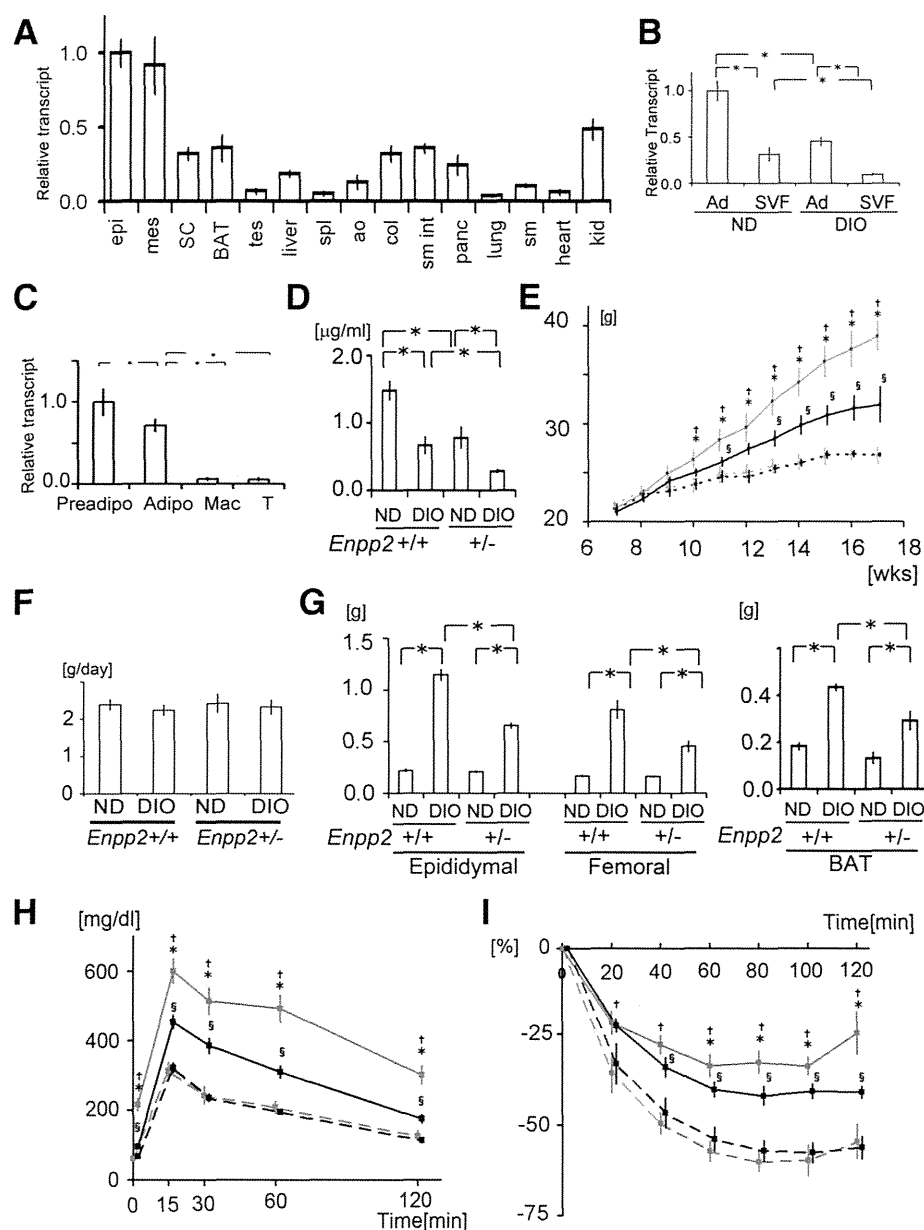
Figure 1—*Enpp2* secreted from adipose tissue contributed to adipose tissue obesity in mice fed a high-fat diet. *A*: Tissue distribution of *Enpp2* mRNA expression in lean WT mice. $n = 5$ animals. epi, epididymal fat pad; mes, mesenteric fat pad; SC, femoral fat pad; tes, testis; spl, spleen; ao, aorta; col, colon; sm int, small intestine; panc, pancreas; sm, skeletal muscle; kid, kidney. *B*: *Enpp2* mRNA expression in the SV fraction (SVF) and adipocyte fraction (Ad) from 20-week-old mice fed an ND and DIO mice. $n = 5$ animals in each group. *C*: *Enpp2* mRNA expression in isolated preadipocytes, adipocytes, macrophages, and T cells from 20-week-old WT mice. $n = 5$ animals in each group. *D–I*: To analyze the role of ENPP2 in adipose tissue obesity, $Enpp2^{+/-}$ and $Enpp2^{+/+}$ mice were fed either an ND or a high-fat diet (DIO) for 10 weeks. All mice were examined when they were 17 weeks old. *D*: Serum ENPP2 levels ($n = 8$ animals in each group). *E*: Body weight changes in $Enpp2^{+/+}$ (gray lines) and $Enpp2^{+/-}$ (black lines) mice fed an ND (broken lines) or a high-fat diet (continuous lines). $n = 8$–10 animals in each group. §$Enpp2^{+/-}$ ND vs. $Enpp2^{+/-}$ DIO; †$Enpp2^{+/+}$ ND vs. $Enpp2^{+/+}$ DIO; *$Enpp2^{+/+}$ DIO vs. $Enpp2^{+/-}$ DIO; $P < 0.05$. *F*: Daily food intake. $n = 8$ animals in each group. *G*: Weights of visceral epididymal, femoral subcutaneous, and interscapular brown fat pads. $n = 8$–10 animals in each group. Results of oral glucose tolerance (1 g/kg glucose) (*H*) and insulin tolerance (1 unit/kg insulin) (*I*) tests in $Enpp2^{+/+}$ (gray lines) and $Enpp2^{+/-}$ (black lines) mice fed an ND (broken lines) or high-fat diet (DIO, continuous lines). §$Enpp2^{+/-}$ ND vs. $Enpp2^{+/-}$ DIO; †$Enpp2^{+/+}$ ND vs. WT DIO; *$Enpp2^{+/+}$ DIO vs. $Enpp2^{+/-}$ DIO. $n = 8$–10 animals in each group. *$P < 0.05$.

Enpp2 Haploinsufficiency Suppresses Adipocyte Hyperplasia in Mice Fed a High-Fat Diet

To begin to elucidate the role played by ENPP2 in obesity, we examined the effects of feeding $Enpp2^{+/-}$ and $Enpp2^{+/+}$ mice a high-fat diet. In $Enpp2^{+/-}$ mice, serum ENPP2 levels were reduced by half (Fig. 1*D*), as were serum and interstitial LPA levels (Supplementary Fig. 1). $Enpp2^{+/-}$ mice fed a high-fat diet showed smaller body weight gains and smaller fat pad weights than $Enpp2^{+/+}$ mice, although food intake did not differ between the two groups (Fig. 1*E*–*G*). Adipocyte numbers in obese epididymal fat pads were smaller in $Enpp2^{+/-}$ diet-induced obese (DIO) mice than in WT DIO mice (Supplementary Fig. 1). In addition, the results of insulin and oral glucose tolerance tests showed that the systemic insulin resistance induced by a high-fat diet was diminished in $Enpp2^{+/-}$ mice (Fig. 1*H* and *I*). ENPP2 deficiency similarly suppressed adipose mass expansion and ameliorated glucose intolerance and insulin resistance in *db/db* mice (Supplementary Fig. 2).

We compared the ectopic fat accumulation in heart, skeletal muscle, and liver using two-photon microscopy (Supplementary Fig. 3). This enabled us to confirm the remarkable fat accumulation seen in all three tissues in $Enpp2^{+/+}$ DIO mice, as compared with $Enpp2^{+/+}$ mice fed a normal diet (ND). Notably, *Enpp2* haploinsufficiency did not affect ectopic fat accumulation in any of these tissues in DIO mice, which ruled out a contribution of ectopic fat to the phenotype of *Enpp2*-deficient mice. Thus, WAT from $Enpp2^{+/-}$ DIO mice showed less expansion, improved metabolism, and less inflammation than WAT from $Enpp2^{+/+}$ DIO mice.

Adipocyte-Expressed ENPP2 Contributes to Adipose Tissue Expansion and Metabolic Dysfunction in DIO Mice

To assess the contribution of ENPP2 produced in adipocytes to the observed phenotype, we selectively deleted the *ENPP2* gene from adipocytes by crossing *Fabp4*-Cre and $Enpp2^{fl/fl}$ mice (Fig. 2 and Supplementary Fig. 4). This deleted ~90, 85, and 80% of *Enpp2* gene from adipocytes in the epididymal, inguinal, and brown fat pads, respectively (Fig. 2*A*). *Ennp2* gene was also deleted by >90% from Pref1⁺ CD34⁺ preadipocytes in epididymal fat pads (Supplementary Fig. 4). Although it has been reported that *Fabp4*-Cre may also drive floxed gene deletion in macrophages and other cell types (18), the overall efficiencies of *Enpp2* deletion from other cell types were <10% in epididymal fat pads in our models.

As in $Enpp2^{+/-}$ mice, serum *Enpp2* levels were reduced by half in adipocyte-specific *Enpp2* KO (Fat-*Enpp2* KO) mice, as compared with WT mice (Fig. 2*B*). In addition, they gained less body weight than control mice when fed a high-fat diet, with no change in food intake (Fig. 2*C* and *D*). The weights of the visceral epididymal, femoral subcutaneous, and interscapular brown fat pads were smaller in Fat-*Enpp2* KO DIO mice than in control

mice (Fig. 2*E*). The numbers of adipocytes in obese epididymal fat pads were smaller in Fat-*Enpp2* KO DIO mice than in WT DIO mice (Supplementary Fig. 4), and Fat-*Enpp2* KO mice showed lower serum triglyceride and cholesterol levels.

Induction of the inflammatory cytokines MCP-1 and TNF-α in epididymal fat pads was diminished in $Enpp2^{+/-}$ DIO mice (Supplementary Fig. 4). Epididymal fat pads from Fat-*Enpp2* KO DIO mice contained fewer CD8⁺ T cells, which reportedly amplify adipose inflammation (10), and fewer Pref1⁺ CD34⁺ preadipocytes and Lin⁻ CD29⁺ CD34⁺ Sca1⁺ progenitors than WT DIO mice (Fig. 2*F*) (19). Following injection of BrdU, the percentage of BrdU⁺ cells among the Pref1⁺ CD34⁺ preadipocytes was smaller in Fat-*Enpp2* KO mice, and the size of the apoptotic preadipocyte cell fraction was increased (Fig. 2*G* and *H*). Expression in epididymal fat of *Lpl* and *CD36(Fat)*, which are involved in fatty acid transport, was lower in Fat-*Enpp2* KO than WT mice (Supplementary Fig. 4), and serum inflammatory cytokine (IL-6, MCP-1, and TNF-α) levels were also lower in $Enpp2^{+/-}$ than $Enpp2^{+/+}$ DIO mice.

Enpp2 Deficiency Improves BAT Function and Increases Energy Expenditure

Adipocyte-specific deletion of *Enpp2* also ameliorated glucose and insulin intolerance induced by a high-fat diet, with no changes in food intake (Fig. 2*D* and Fig. 3*A* and *B*). Our finding that *Enpp2* deficiency reduces fat pad expansion in WAT and BAT and improves systemic metabolism prompted us to examine locomotion and EE. We found that the body weights of mice fed a high-fat diet were increased after 10 weeks but were unchanged after 4 weeks (Fig. 2*C*). On the other hand, an increase in EE was observed in Fat-*Enpp2* KO DIO mice after as little as 4 weeks on the high-fat diet (Fig. 3*C*–*F* and Supplementary Fig. 4), and Fat-*Enpp2* KO DIO mice exhibited greater spontaneous locomotive activity than WT DIO mice after 10 weeks on a high-fat diet (Fig. 3*G* and *H*). This suggests increased EE was at least partially responsible for the smaller body weight gain seen in *Enpp2* KO DIO mice.

The expression of *Enpp2* in BAT and the contribution of *Enpp2* deficiency to improved systemic metabolism prompted us to analyze BAT functionality in these mice. Imaging BAT tissue in WT DIO mice revealed that nearly 30% of adipocytes showed multiple lipid droplets, a morphological feature of functional brown adipocytes, whereas the other adipocytes contained single lipid droplets (Fig. 3*I*). By contrast, the number of adipocytes containing multiple lipid droplets was increased to ~70% in Fat-*Enpp2* KO DIO mice. We therefore speculated that the number of functional brown adipocytes was increased in Fat-*Enpp2* KO DIO mice. In addition, mitochondrial content is increased in BAT from both ND and DIO Fat-*Enpp2* KO mice (Supplementary Fig. 5). The thermogenic function of BAT under cold conditions was improved in Fat-*Enpp2* KO DIO mice, as compared with WT DIO mice